Brain, Behavior, & Immunity - Health 38 (2024) 100780

Contents lists available at ScienceDirect

Brain, Behavior, & Immunity - Health

journal homepage: www.editorialmanager.com/bbih/default.aspx

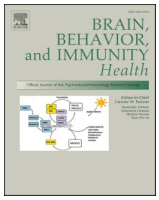

Arbovirus infection increases the risk for the development of neurodegenerative disease pathology in the murine model

Chanida Fongsaran [a,b,c], Krit Jirakanwisal [a,b,c], Bi-Hung Peng [d], Anna Fracassi [e], Giulio Taglialatela [c,e], Kelly T. Dineley [e,f], Slobodan Paessler [a,b], Irma E. Cisneros [a,b,c,f,*]

[a] Department of Pathology, University of Texas Medical Branch, Galveston, TX, USA
[b] Institute for Human Infections and Immunity, University of Texas Medical Branch, Galveston, TX, USA
[c] Neuroinfectious Diseases, University of Texas Medical Branch, Galveston, TX, USA
[d] Department of Neurobiology, University of Texas Medical Branch, Galveston, TX, USA
[e] Mitchell Center for Neurodegenerative Diseases, Department of Neurology, University of Texas Medical Branch, Galveston, TX, USA
[f] Center for Addiction Sciences and Therapeutics, University of Texas Medical Branch, Galveston, TX, USA

ARTICLE INFO

Keywords:
VEEV
TC-83
Alphavirus
Neuroinflammation
Alzheimer's disease

ABSTRACT

Alzheimer's disease is classified as a progressive disorder resulting from protein misfolding, also known as proteinopathies. Proteinopathies include synucleinopathies triggered by misfolded amyloid α-synuclein, tauopathies triggered by misfolded tau, and amyloidopathies triggered by misfolded amyloid of which Alzheimer's disease (β-amyloid) is most prevalent. Most neurodegenerative diseases (>90%) are not due to dominantly inherited genetic causes. Instead, it is thought that the risk for disease is a complicated interaction between inherited and environmental risk factors that, with age, drive pathology that ultimately results in neurodegeneration and disease onset. Since it is increasingly appreciated that encephalitic viral infections can have profoundly detrimental neurological consequences long after the acute infection has resolved, we tested the hypothesis that viral encephalitis exacerbates the pathological profile of protein-misfolding diseases. Using a robust, reproducible, and well-characterized mouse model for β-amyloidosis, Tg2576, we studied the contribution of alphavirus-induced encephalitis (TC-83 strain of VEEV to model alphavirus encephalitis viruses) on the progression of neurodegenerative pathology. We longitudinally evaluated neurological, neurobehavioral, and cognitive levels, followed by a post-mortem analysis of brain pathology focusing on neuroinflammation. We found more severe cognitive deficits and brain pathology in Tg2576 mice inoculated with TC-83 than in their mock controls. These data set the groundwork to investigate sporadic Alzheimer's disease and treatment interventions for this infectious disease risk factor.

1. Introduction

Alphaviruses are arthropod-transmitted, enveloped, positive-sense, single-stranded RNA viruses segregated into Old or New World groups (Peiris et al., 1994). Old World alphaviruses, such as Chikungunya, O'nyong-nyong, and Ross River viruses, are commonly found in Europe, Asia, Australia, and/or Africa and cause acute febrile illness followed by arthralgia in animal and human hosts (Aguilar et al., 2011). New-world alphaviruses, such as Venezuelan equine encephalitis (VEE), eastern equine encephalitis (EEE), and western equine encephalitis (WEE) viruses, are spread within the Americas and result in up to 90% of survivors exhibiting encephalitis and neurological sequelae (Mulder et al., 1951; Rivas et al., 1997; Ronca et al., 2016) (see Schemes 1 and 2).

Evidence suggests infections with neurotropic pathogens, including alphaviruses, contribute to the development of neurodegenerative diseases (Onisiforou and Spyrou, 2021). For example, WEEV infection in a rodent model leads to glial cell activation and acute and chronic loss of dopaminergic neurons in the substantia nigra pars compacta (Bantle et al., 2019). Interestingly, phospho-serine129 α-synuclein positive, proteinase K-resistant protein aggregates are also present, indicating neurological sequelae and neuronal injury consistent with Parkinson's neurodegenerative phenotype (Bantle et al., 2019). In a mouse model of VEEV encephalitis, mice displayed behavioral and neuropathological phenotypes associated with several neurological disorders, including

* Corresponding author. Department of Pathology, University of Texas Medical Branch, Galveston, TX, USA.
E-mail address: ircisner@utmb.edu (I.E. Cisneros).

https://doi.org/10.1016/j.bbih.2024.100780
Received 20 November 2023; Received in revised form 4 March 2024; Accepted 23 April 2024
Available online 24 April 2024

schizophrenia, Alzheimer's disease (AD), and autism spectrum disorders (Ronca et al., 2017). South and Central American outbreaks of VEEV produce a highly virulent central nervous system (CNS) disease in horses and other equines (Schoneboom et al., 2000). In humans, VEEV typically leads to flu-like illness, ranging from mild to severe encephalitis and neurological symptoms such as seizures, drowsiness, and confusion (Weaver et al., 2004). Neurological complications may occur in 4–14% of symptomatic cases (Gardner et al., 2008). VEEV can progress to a neurological disease characterized by edema, meningitis, and congestion due to mononuclear inflammatory infiltrates (Ehrenkranz and Ventura, 1974). Similar symptoms have been found in preclinical rodent models. For example, in the C3H/HeN mouse strain, primary clinical indicators of VEEV TC-83 infection typically encompass weight loss, hunching, and fluctuations in alertness/lethargy, culminating in mice eventually progressing to a moribund state (Julander et al., 2008). It infects neurons and glial cells in the CNS, promoting neurodegeneration and potentially leading to permanent neurological sequelae during its lymphotropic and neurotropic phases (Bocan et al., 2019; Gleiser et al., 1962; Schoneboom et al., 2000). VEEV infection causes gliosis and neuroinflammation, indicating indirect mechanisms of neuronal degeneration, like neurotoxic mechanisms related to AD (Schoneboom et al., 2000). Furthermore, increased and chronic production of pro-inflammatory cytokines in the CNS results in neurological sequelae and possible development of permanent neuronal damage and death.

VEEV neuropathology shares similarities with AD, a widespread cognitive disorder of aging, including increased astrogliosis, glial nodules, and pathological indicators of neuroinflammation including perivascular cuffing (Nelson et al., 2012; Williams et al., 2023). Over the past 25 years, progress within the aging and dementia research community has continued, identifying risk factors and characterizing AD's clinical and pathologic features (Tarawneh and Holtzman, 2012). Thus, a reconceptualization of AD suggests a long asymptomatic phase during which significant pathology starts to develop (e.g., amyloid accumulation, synaptic damage) prior to potentially prodromal phase as well as clinically symptomatic cognitive impairment (Sperling et al., 2011). Sporadic (idiopathic) AD is slowly progressive and the most common cause of dementia in those aged 65 and older making more than 90% of the disease cases (Geschwind et al., 2007). In sporadic AD, genetic and environmental risk factors contribute to impaired amyloid beta (Aβ) clearance and abnormal Aβ accumulation in the brain, triggering the pathophysiology of early AD, including synaptic dysfunction, synaptic loss, and progressive memory deficits. Notwithstanding the role of aging in AD, environmental risk factors are suspected but unproven in exacerbating the disease (Sochocka et al., 2017). Identifying causative agents and understanding AD etiology will be highly informative from a risk assessment standpoint. Given that encephalitic viral infections can have profoundly detrimental neurological consequences long after acute infection has resolved, it is logical that encephalitic viral infections, such as alphaviral infection, may exacerbate the onset and neuropathology of AD. However, whether encephalitic viral infections provide a causative link in initiating the development of AD remains unknown.

Here, we test if alphavirus encephalitis will exacerbate AD cognitive deficits and Aβ related neuropathology in an animal model for Aβ amyloidosis. Although there are no current vaccines for VEEV in the United States, a live-attenuated and formalin-inactivated version of VEEV is used by the US military and laboratory workers (Stromberg et al., 2020; K. Taylor, Kolokoltsova, Ronca, Estes and Paessler, 2017a). TC-83, an attenuated VEEV strain, induces neurological sequelae in a mouse model for VEEV neurological sequelae and allows researchers to work at lower biocontainment level to study virus-induced behavioral changes as well as CNS inflammation (K. Taylor, Kolokoltsova, Ronca, Estes and Paessler, 2017b). Thus, utilizing the Tg2576 mouse, a preclinical rodent model genetically programmed to overproduce Aβ, we expect to exacerbate hippocampus-dependent memory impairments, heightened neuroinflammation, gliosis, and neuropathology in parallel to aberrant Aβ accumulation, which is common between this model and sporadic AD. Furthermore, the Tg2576 phenotype overlaps with currently accepted biomarkers for early AD pathophysiology in humans. Most importantly, the model exhibits progressive cognitive decline and AD-like pathology. However, neither profound neuroinflammation nor neurodegeneration is evident, suggesting that additional sequelae are necessary to manifest the complete disease profile. We anticipate that results from this study will support the infectious etiology hypothesis of AD.

2. Material and methods

2.1. Cells, viruses, and biosafety

Vero E6 (ATCC® CRL-1586™) were maintained in Dulbecco's modified Eagle's medium (DMEM) supplemented with 10% fetal bovine serum (FBS) and 1% penicillin-streptomycin. VEEV TC-83 stocks were generated by growth in cell culture and viral titer of the stock was obtained via plaque assay, as described previously (Paessler et al., 2008). All work with infectious viruses was performed at the University of Texas Medical Branch (UTMB) A/BSL-2 in accordance with institutional health and safety guidelines and behavioral studies were conducted in ABSL3 to access the equipment in that facility.

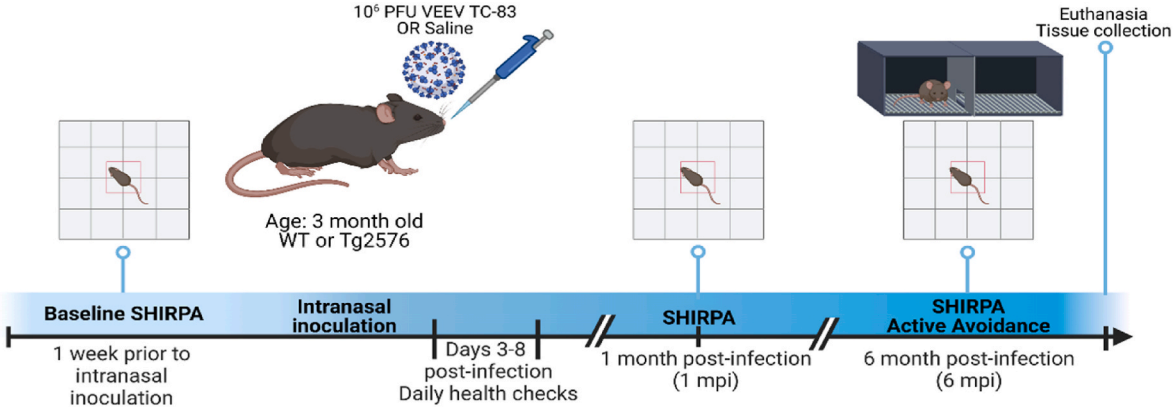

Schematic 1. Experimental design. Wild-type (WT-B6SJL) and transgenic Tg2576 (B6SJL-Tg [APPSWE]), 3-month-old mice performed baseline SHIRPA examinations 1 week prior to intranasal inoculation with VEEV TC-83 (10^6 PFU). During the acute phase of infection (0–8 days post-inoculation [dpi]), mice were weighed, and temperatures were checked daily. At 1 and 6 mpi, SHIRPA was reevaluated. At 6 mpi, mice performed active avoidance training, immediately followed by euthanasia and tissue collection for downstream biochemistry. WT saline *(n = 8)*; WT VEEV TC-83 *(n = 9)*; Tg2576 saline *(n = 8)*; Tg2576 VEEV TC-83 *(n = 8)*. Created with BioRender.com.

2.2. Animal experiments

The mice, Tg2576, were bred in the UTMB Animal Care Facility by mating heterozygous Tg2576 male with wild-type (WT, C57BL6/J x SJL/J) F_1 female mice (The Jackson Laboratory). UTMB complies with the U.S. Department of Agriculture Animal Welfare Act, the Guide for the Care and Use of Laboratory Animals, and Institutional Animal Care and Use Committee (IACUC)-approved protocols. Mice were housed (n < 5/cage) with food and water *ad libitum*. All animal manipulations were conducted during the lights-on phase (0700–1900). Prior to intranasal inoculation, three month old WT male ($n = 8$), WT female ($n = 9$), Tg2576 male ($n = 10$), and Tg2576 female ($n = 6$) mice were anesthetized using isoflurane precisions variable-bypass vaporizer. As soon as the mice lost consciousness and started to hyperventilate, they were inoculated with 10^6 PFU VEEV TC-83 diluted in PBS, or PBS alone as mock control in a total volume of 20 µl and were pipetted as intranasal drops noninvasively to alternating nares until all 20 µl were delivered. Mice were observed daily and weights/temperatures measured, during the acute phase of infection, for signs of disease, until eight day post-inoculation (dpi) and the mortality was checked daily throughout the experiment. Standardized recording of death and clinical outcomes were scored attributed to lethargy, reduced activity, development of discoordination, ataxia, and/or paralysis. The sample size for sex were not enough to stratify data based on sex, thus sex was collapsed for all analysis.

2.3. General health assessment

A modified SHIRPA screen was used to analyze the general health of each animal pre- and post-infection (Rogers et al., 1997). Semi-quantitative measurements were performed to evaluate body position, spontaneous activity, respiratory rate, touch escape, transfer arousal, gait, piloerection, visual placing, trunk curl, and fear (Table 1). Semi-quantitative measurements were ranked on a scale from "zero" to "three", with "zero" being the lowest possible, "one" equating to less than normal, "two" equating to normal, and "three" equating to hyperactive. Animals were transferred from their home cage to a Perspex jar and allowed to acclimate for 5 min. Observation of body position was scored based on whether the mouse was flat, prone, sitting/standing, or repeatedly leaping. Respiratory rate was scored as irregular, shallow, normal, or overactive. Additional observations included clinically abnormal observations, including hunched-back and grooming behaviors. Following 5 min observation, mice were dropped into an open field arena from approximately 30 cm above. Transfer arousal, also described as movement type, was evaluated for coma-like, prolonged freeze, momentary freeze followed by swift movement, or extremely excited. Spontaneous activity was determined by observing the mouse during the exploratory phase and evaluating whether the mouse movement was immobile, slow, moderate, or vigorous. We evaluated piloerection on whether the mouse coat was on end or not. The gait of the mouse was assessed based on whether it was fluid but abnormal, limited, normal, or incapacity. Next, we would approach the mouse with forceps and evaluate whether the mouse attempted to escape touch based on whether the mouse had no response, mild response, normal moderate response, or vigorous attempts to escape. The mice were then lifted by the tail with forceps, and visual placing was evaluated for absence before vibrissae contact, at vibrissae contact, or a vigorous extension. Trunk curl was determined to be absent, struggling, present, or too hyperactive to perform. Lastly, the fear of the animal was observed and evaluated based on whether the mouse would lightly freeze, moderately freeze, not freeze, or was hyperactive to the new environment and the investigator performing the assays. The assays were slightly modified but mostly

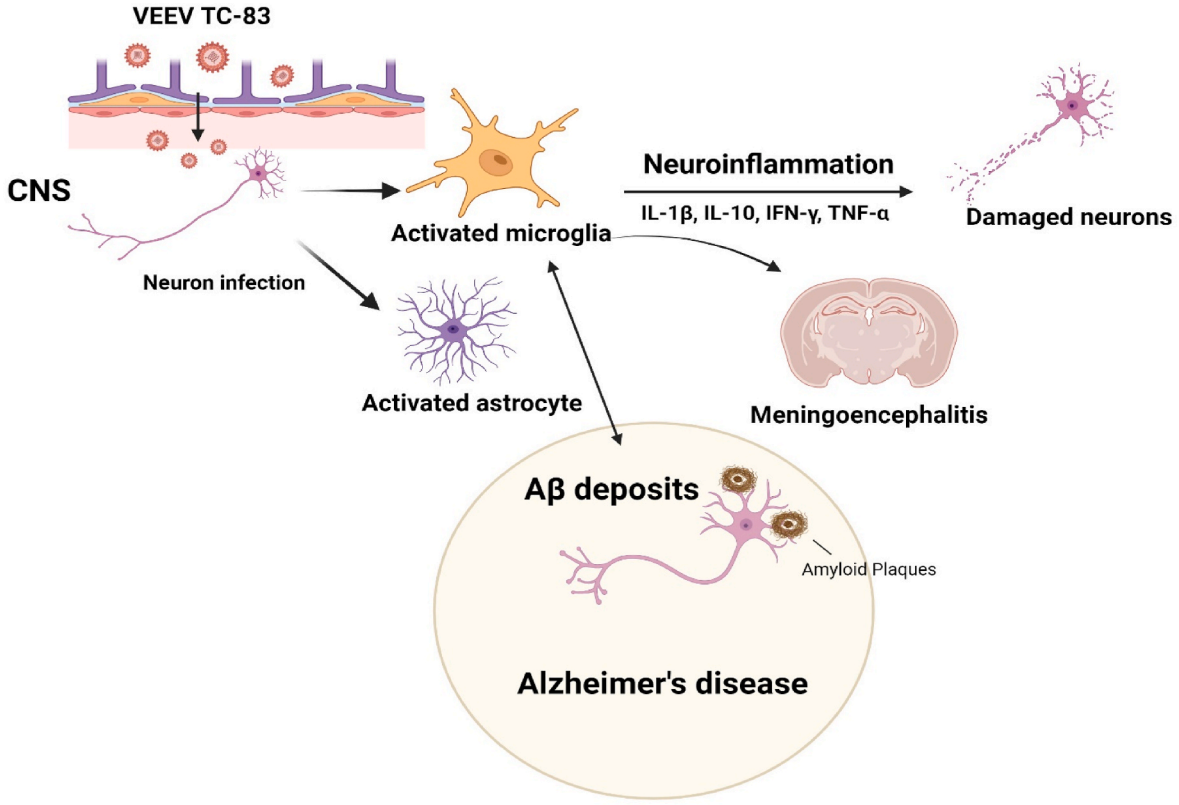

Schematic 2. The graphical interactions between VEEV TC-83 and Alzheimer's Disease (AD). VEEV TC-83 is associated with pro-inflammatory states, promoting the secretion of cytokines such as IL-1β, IL-10, IFN-γ, and TNF-α. This cascade of inflammatory responses can potentially lead to neuronal damage or dysfunction, exacerbating the pathogenesis of AD. Moreover, VEEV TC-83 increases the risk for amyloid-beta plaque formation, a main hallmark observed in the brains of AD. Created with BioRender.com.

Table 1
Modified SHIRPA evaluations and scores.

Categories	Observations	Responses	Scores
Autonomic Function			
	Respiration Rate	Overactive	3
		Normal	2
		Shallow	1
		Irregular	0
	Piloerection	Normal	2
		Coat was on end	1
Motor Behavior			
	Body position	Overactive	3
		Sitting/Standing	2
		Prone	1
		Flat	0
	Gait	Fluid but abnormal	3
		Normal	2
		Limited	1
		Incapacity	0
	Trunk Curl	Hyperactive	3
		Present	2
		Struggling	1
		Absent	0
Reflex & Sensory Function			
	Visual Placing	Vigorous extension	3
		Vibrissae contact	2
		Before vibrissae contact	1
		Absent	0
Neuropsychiatric State			
	Spontaneous	Vigorous	3
	Activity	Moderate	2
		Limited	1
		Immobile	0
	Transfer arousal	Extremely excited	3
		Freeze followed by swift movement	2
		Prolonged freeze	1
		Coma-like	0
	Touch escape	Vigorous attempts to escape	3
		Normal moderate response	2
		Mild response	1
		No response	0
	Fear	Hyperactive	3
		Moderate freeze	2
		Lightly freeze	1
		No freeze	0

performed as previously described (Lalonde et al., 2021; Rogers et al., 2001; Zhang et al., 2016). We established baseline SHIRPA one week prior to inoculation. Post-inoculation measurements were evaluated beginning one month post-inoculation (mpi) through the end of the study at 6 mpi (**Schematic 1**).

2.4. Active avoidance

Active avoidance testing was performed at 6 mpi, in WT and Tg2576, saline inoculated and VEEV TC-83 inoculated male and female mice, to evaluate their ability to learn using classic Pavlovian conditioning. The mice were removed individually from their home cages and placed into the Ugo Basile shuttle box, housed within biosafety cabinet. The mice were stimulated with a sound (90–100 dB) and light (conditioned stimulus) for 10 s. Mice not moving to the other chamber during the conditioned stimulus received a shock (0.3 mA) for up to 4 s (unconditioned stimulus). The mouse was allowed to escape the shock during these 4 s. Mice performed 30 trials consecutively for three days. The number of avoidances, escapes, and the latency for avoidances and escapes were recorded. Mice that did not attempt to cross during the unconditioned stimulus five trials in a row were removed from the shuttle box and did not perform additional trials that day.

2.5. RNA and protein extraction

At the conclusion of the study (6 mpi), mice were euthanized with carbon dioxide, followed by cervical dislocation. Brain was rapidly extracted, flash-frozen in liquid nitrogen, and stored at −80 °C until processing. Tissue was homogenized using the TissueLyser II (Qiagen) for 60 s at a speed of 3 m/s in 200–500 μL ice-cold homogenization/extraction buffer (20 mM HEPES, 200 mM NaCl, 1 mM EDTA, 1 mM DTT, 10 μL/mL phosphatase inhibitor cocktail 2 [Sigma, Cat #P5726], 10 μL/mL phosphatase inhibitor cocktail 3 [Sigma, Cat #P0044], RNase inhibitor). Homogenized samples were aliquoted for RNA and protein isolation. The homogenate was centrifuged at 14,000×*g* for 5 min at 4 °C, and the supernatant was transferred to a new tube. The total RNA was prepared using a standardized TRIzol reagent (Invitrogen) protocol. The RNA amount was assessed using Nanodrop equipment (DeNovix DS-11+Spectrophotometer). The protein amount was measured using a Precision Red, Advance Protein Assay Reagent #2 (Cytoskeleton, Inc. Denver, CO, USA) following the manufacturer's instructions.

2.6. Real-time PCR

First-strand cDNA was synthesized using the High-Capacity cDNA Reverse Transcription Kits (Applied Biosystems) according to the manufacturer's protocol. One microliter of cDNA templates (2 mg) was added to triplicate 20 μl reaction mixtures with TaqMan® Fast Advanced Master Mix and primers (Cat #4444557, Applied Biosystems, Foster City, CA). Quantitative PCR was then performed by StepOnePlus™ Real-Time PCR System (Applied Biosystems) using Taqman primer-probe sets and Taqman reagents. The primer-probe sets used were mouse IL-10 (Mm00439616_m1), TNF-α (Mm00443258_m1), IFN-γ (Mm01168134_m1) and rat IL-1β (Rr00580432_m1) with an 88.275 gene alignment with mouse IL-1β. The thermal profile was as follows: 95 °C for 2 min of initial denaturation followed by 40 cycles of 95 °C for 1 s to denature and 60 °C for 20 s to anneal and extend. The housekeeping gene, glyceraldehyde-3-phosphate dehydrogenase (GAPDH, Mm99999915_g1), was used as an internal control. Data were analyzed by calculating the $2^{-\Delta\Delta Ct}$ for the differences between the VEEV TC-83 and control groups. Sex was collapsed.

2.7. Histopathology and immunofluorescence staining

The brains of mice euthanized at 6 mpi were dissected and fixed with 10% neutral buffered formalin overnight in the UTMB BSL-3 facility to allow for appropriate agent inactivation. After formalin fixation, brain samples were embedded in paraffin, and sections were cut at 5 μm onto slides by the Research Histology Laboratory Core at UTMB. The slides were processed for both hematoxylin and eosin (H&E) and immunofluorescence staining. The H&E slides were imaged using Olympus IX73 inverted microscope, Olympus DP80 digital camera, and Olympus cellSens imaging software. The sections were deparaffinized for immunofluorescence using xylene and graded ethanol and rehydrated. Slides were then immersed in 10 mM sodium citrate buffer, pH 6.1 (Vector Laboratories H-3300, Newark, CA, USA) and processed for the antigen retrieval procedure using a microwave oven operated at 640 W for 10 min. After cooling for 1 min, slides were transferred to a new antigen retrieval solution, following the same procedure. After cooling at room temperature for 30 min, slides were washed in PBS for 5 min. Nonspecific binding sites were blocked with 5% bovine serum albumin (BSA) (catalog# A4503-100G, Sigma-Aldrich)/10% normal goat serum (NGS, catalog# S26-100 mL Sigma-Aldrich) and serial sections were permeabilized with 0.2% Triton X-100 for 1 h at room temperature. Slides were incubated with the following primary antibodies, diluted in PBS containing 1.5% NGS/overnight at 4 °C: rabbit anti-Iba1 (1:200, catalog#19741, FUJIFILM Wako); chicken anti-GFAP (1:500; catalog# GFAP, Aves Labs); mouse anti-Aβ (1:100, catalog# 803,001, Biolegend). Slides were washed in PBS before incubation with the appropriate Alexa-conjugated secondary antibodies (goat anti-rabbit Alexa Fluor 488, 1:400, catalog# A-11008; goat anti-mouse Alexa Fluor 594, 1:400 catalog# A-11032; goat anti-chicken Alexa Fluor 647, 1:400, catalog# A-

21449, ThermoFisher Scientific) in PBS containing 1.5% NGS for 1 h at RT. Finally, slides were washed in PBS, treated with 0.3% Sudan Black B prepared in 70% EtOH for 10 min to block lipofuscin autofluorescence, rewashed with deionized water, and coverslipped using Fluoromount-G containing 4′,6-diamidino-2-phenylindole (DAPI) (Cat# 0100–20, SouthernBiotech) and sealed.

2.8. Quantitative microscopy

All immunoreacted sections were acquired with a Keyence BZ-X800 (Keyence Corporation) microscope using 20*x* and 40*x* objectives. For all analyses, each animal was analyzed as previously described (Fracassi et al., 2023). The mouse brains were utilized with sagittal, cross-sectional, serial dimensions. Briefly, an average of three sections were analyzed for each animal/area (CA1, CA3, DG), and images were taken at 1920 × 1440 pixel resolution, with z-step size of 0.5 at 5 μm thickness. For the feasibility of the quantification, all layers from a single image stack were projected on a single slice (stack/Z projection). Quantitative analyses were performed using ImageJ software (https://imagej.nih.gov/ij, NIH). We analyzed the fluorescence intensity for Iba1, GFAP, and Aβ per area (Integrated Density, IntDen). Representative images were composed in an Adobe Photoshop CC2020 format.

2.9. Enzyme-linked immunosorbent assay (ELISA)

ELISA for Amyloid β peptide 1–40 (Cat # MBS7725105; MyBioSource, San Diego, CA) and Amyloid β peptide 1–42 (Cat # MBS7724636, MyBioSource, San Diego, CA) were performed according to the manufacturer's instructions. Briefly, equal concentrations of protein (30 μg) and standards were added into pre-coated 96-well plates and then incubated for 1 h at 37 °C. Plates were subsequently washed, and Detection reagent B was added to each well for 30 min, followed by substrate and stop solution. The enzymatic reaction was quantified by measuring absorbance at 450 nm using a GloMax Discover Microplate reader (Promega, Madison, WI).

2.10. Statistical analysis

Statistics were performed using GraphPad Prism (version 9.3.1). Normal distribution was tested using the Shapiro-Wilk test. For analyzing the differences in normally distributed data with multiple groups, comparisons were performed using a one-way analysis of variance (ANOVA) followed by Tukey post-hoc analysis; or two-way ANOVA, or mixed effects model, Geisser-Greenhouse correction, followed by Tukey post-hoc analysis. To compare two groups, we used an independent sample *t*-test, followed by Tukey post-hoc test. All data are reported as mean ± SEM. A significance level of $p < 0.05$ at 95% confidence intervals was considered statistically significant for all the experiments reported in this study.

3. Results

3.1. VEEV TC-83 inoculation differentially impacts disease severity in WT and Tg2576 mice

To evaluate disease symptoms mediated by VEEV TC-83, we

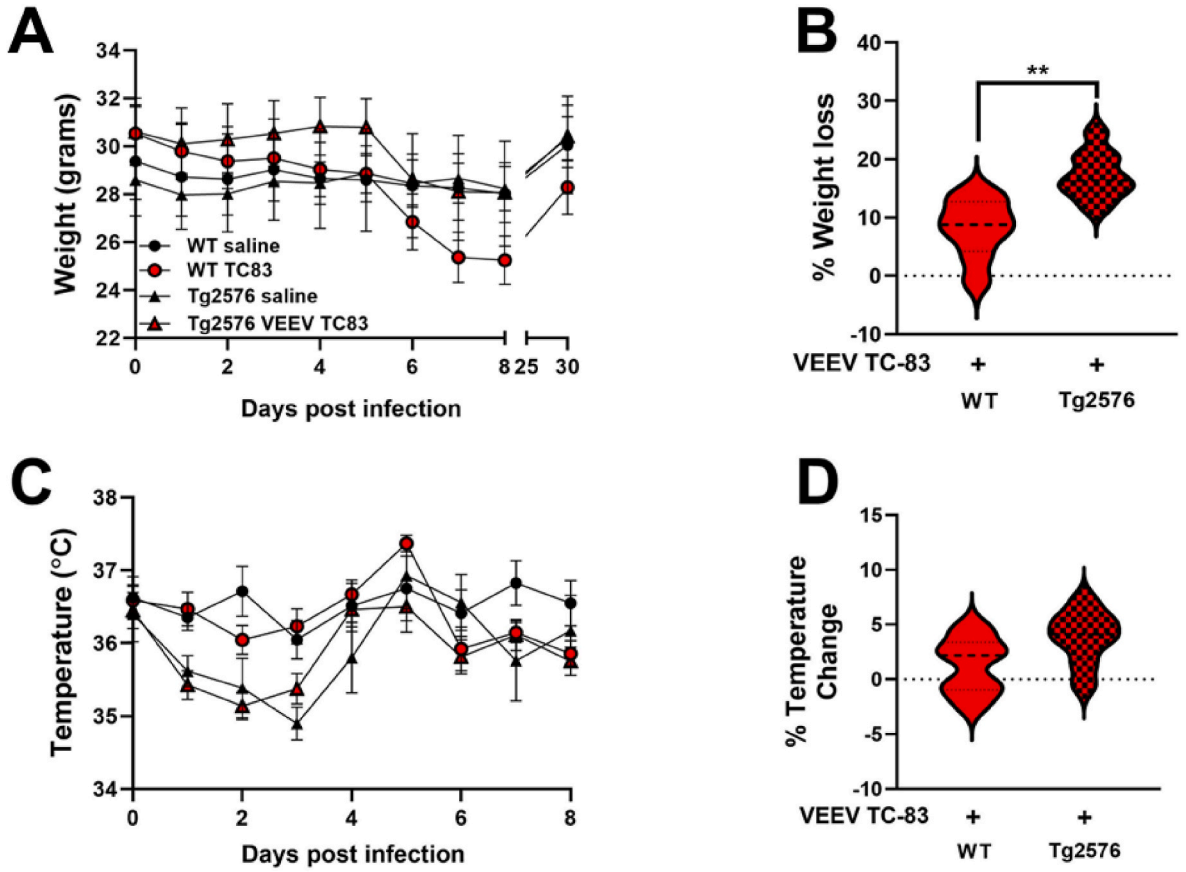

Fig. 1. Acute weight and temperature changes following VEEV TC-83 inoculation. Weight and temperature changes were measured in WT saline ($n = 8$), WT VEEV TC-83 ($n = 9$), Tg2576 Saline ($n = 8$), and Tg2576 VEEV TC-83 ($n = 8$) mice directly before and during acute challenge with VEEV TC-83 (A and C). Percent weight loss was calculated at 8 dpi in WT VEEV TC-83 and Tg2576 VEEV TC-83 mice (B). Percent temperature change was calculated in WT VEEV TC-83 and Tg2576 VEEV TC-83 mice (D). Statistical analyses were measured by a two-tailed, unpaired, parametric *t*-test with a 95% confidence interval. Values are expressed as the mean ± SEM. $^{**}p < 0.01$.

measured weight and temperature changes daily during the acute phase of infection (0–8 days post-inoculation). A downward trend in weight loss was measured in Tg2576 mice inoculated with VEEV TC-83 over the course of eight days post-inoculation (dpi); however, the weights of all mice recovered at 30 dpi, regardless of VEEV TC-83 exposure (Fig. 1A). A larger percentage of weight loss was measured in Tg2576 mice inoculated with VEEV TC-83 ($n = 8$) when compared to WT VEEV TC-83 inoculated mice ($n = 8$, $^{**}p < 0.01$, Fig. 1B), suggesting that the Tg2576 genotype contributes to disease related symptoms. No differences in temperature were detected between the groups (Fig. 1C). No significant changes in temperature were quantified between WT VEEV TC-83 inoculated, and Tg2576 VEEV TC-83 inoculated mice (Fig. 1D).

3.2. VEEV TC-83 exposure exacerbates sensorimotor function and emotional reactivity in Tg2576-mice

To evaluate the impact of VEEV TC-83 exposure on motor activity, coordination, and emotional reactivity, baseline SHIRPA assessments were performed prior to inoculation with VEEV TC-83 (Supplemental Table 1). Repeated SHIRPA assessments were longitudinally measured at one-month post-inoculation (mpi) (Table 2) and 6 mpi (Table 3). Amongst the assessments with abnormal responses, body position, spontaneous activity, respiratory rate, touch escape, transfer arousal, gait, piloerection, visual placing, trunk curl, and fear were measured. At 1 mpi, 50% or greater (shaded boxes) of WT-inoculated mice had abnormal responses in three categories: spontaneous activity, touch response, and transfer arousal (Table 2). At 6 mpi, most WT-inoculated mice recovered; zero categories had 50% or greater WT-inoculated mice display abnormal responses (Table 3). At 1 mpi, more than 50% of Tg2576 mice inoculated with VEEV TC-83 displayed abnormal responses in nine categories: body position, spontaneous activity, respiratory rate, touch escape, transfer arousal, gait, visual placing, trunk curl, and fear (Table 2). At 6 mpi, Tg2576 inoculated mice continued to have 50% or greater abnormal responses in seven categories but recovered in respiratory rate and gait (Table 3). Taken together, exposure to VEEV TC-83 triggered the development of abnormal responses, despite genotype, at 1 mpi that recovered in WT mice at 6 mpi ($^{*}p < 0.05$, $^{***}p < 0.01$, Fig. 2A and B). However, longitudinal evaluations reveal that Tg2576 mice, inoculated with VEEV TC-83 continued to have exaggerated neurological abnormalities compared to WT VEEV TC-83 inoculated mice ($^{**}p < 0.01$, $^{***}p < 0.001$, Fig. 2B), supporting the infectious etiology hypothesis of AD.

3.3. VEEV TC-83 inoculated mice have an increased latency to avoid and escape shock

To evaluate the impact of VEEV TC-83 infection on neurological sequelae and behavioral learning deficits, Pavlovian fear or threat conditioning (Diehl et al., 2019; Salah et al., 2021) using standard two-way active avoidance was performed. During three days of active avoidance testing, we found no significant differences in the number of avoidance or escape attempts performed between the four groups (Fig. 3A and B). However, we quantified significant differences in the latency to avoid shock in Tg2576 mice inoculated with VEEV TC-83 (Fig. 3C). Using a mixed effects analysis, we found a significant effect between the days of testing ($^{*}p < 0.05$, $F[1.856, 57.55] = 4.627$), and VEEV TC-83 inoculation ($^{***}p < 0.001$, $F[3, 62] = 39.76$) on latency to avoid shock, but no significant interaction between days of testing and VEEV TC-83 inoculation (ns, $F[6, 62] = 0.9341$; Fig. 3C). In parallel, we found no differences between days of testing (ns, $F[1.898, 53.15] = 2.105$) in latency to escape shock; however, VEEV TC-83 inoculation significantly impacted the latency to escape shock ($^{***}p < 0.001$, $F[3, 29] = 26.74$) and a significant interaction was found between VEEV TC-83 inoculation and the days tested ($^{*}p < 0.05$, $F[6, 56] = 2.538$) (Fig. 3D). Performing a multiple comparisons analysis, we found no differences in the latency to avoid or escape shock in WT mice inoculated with VEEV TC-83 compared to their saline controls (Fig. 3C and D); however, VEEV TC-83 inoculation in Tg2576 mice, significantly increased the time it took for them to avoid or escape shock compared to Tg2576 saline mice, despite the day of testing ($^{*}p < 0.05$, $^{**}p < 0.01$, $^{***}p < 0.001$, Fig. 3C and D). Taken together, this suggests that VEEV TC-83 exposure does impact the ability for AD phenotypes to learn and retain events.

3.4. VEEV TC-83 inoculation produces altered CNS inflammatory cytokine profiles

To determine changes in CNS inflammatory cytokine gene expression following VEEV TC-83 inoculation in WT and Tg2576 mice, levels of interleukin (IL)-1β, IL-10, tumor necrosis factor (TNF)-α and interferon (IFN)-γ were quantified in total brain homogenates at 6 mpi. In saline inoculated WT mice, no detectable levels of IL-1β were measured; however, IL-1β levels were detected in saline-inoculated Tg2576 mice and an increase in IL-1β levels were quantified in WT inoculated mice (Fig. 4A). Significantly higher levels of IL-1β were measured in Tg2576 mice, inoculated with VEEV TC-83, when compared to saline-inoculated Tg2576 ($^{**}p < 0.01$, Fig. 4A). No significant differences were quantified in anti-inflammatory cytokine, IL-10, in any groups (Fig. 4B). Levels of CNS TNF-α significantly increased in WT animals following infection with VEEV TC-83 compared to WT saline mice ($^{*}p < 0.05$, Fig. 4C). VEEV TC-83 inoculated Tg2576 mice expressed significantly higher levels of TNF-α, compared to both WT VEEV TC-83 and Tg2576 saline mice ($^{**}p < 0.01$, $^{***}p < 0.001$, Fig. 4C). Lastly, we quantified a significant increase in IFN-γ in Tg2576 mice inoculated with VEEV TC-83 compared to Tg2576 saline mice and to WT-inoculated mice ($^{*}p < 0.05$, $^{***}p < 0.001$, Fig. 4D). Taken together, this indicates that VEEV

Table 2
SHIRPA scores. At 1 mpi, mice performed SHIRPA. SHIRPA responses were scored on a scale of 0–3 (0 = no response, 1 = slow response; 2 = normal response; 3 = hyper response). Ratios show the number of mice with normal (Score of 2) versus abnormal scores (Score of 0, 1, or 3) (normal/abnormal) between each group and for each individual SHIRPA response. Abnormal percentages were calculated for each group and for each SHIRPA response tested. Shaded boxes are SHIRPA responses with 50% or greater abnormal responses.

SHIRPA Response	Body position	Spontaneous activity	Respiratory rate	Touch escape	Transfer arousal	Gait	Piloerection	Visual placing	Trunk curl	Fear
WT Saline	8/0	6/2	8/0	6/2	6/2	8/0	8/0	8/0	5/3	8/0
Tg2576 Saline	8/0	5/3	7/1	5/3	5/3	8/0	8/0	8/0	5/3	6/2
WT VEEV TC-83	7/2	4/5	9/0	4/5	4/5	5/4	6/3	7/2	5/4	7/2
Tg2576 VEEV TC-83	3/5	3/5	2/6	0/8	0/8	4/4	6/2	3/5	3/5	0/8
Abnormal Percentage										
WT Saline	0%	25%	0%	25%	25%	0%	0%	0%	37.5%	0%
Tg2576 Saline	0%	37.5%	12.5%	37.5%	37.5%	0%	0%	0%	37.5%	25%
WT VEEV TC-83	22.2%	55.5%	0%	55.5%	55.5%	44.4%	33%	22.2%	44.4%	22.2%
Tg2576 VEEV TC-83	62.5%	62.5%	75%	100%	100%	50%	25%	62.5%	62.5%	100%

Table 3
SHIRPA scores. At 6 mpi, mice performed SHIRPA. SHIRPA responses were scored on a scale of 0–3 (0 = no response, 1 = slow response; 2 = normal response; 3 = hyper response). Ratios show the number of mice with normal (Score of 2) versus abnormal scores (Score of 0, 1, or 3) (normal/abnormal) between each group and for each individual SHIRPA response. Abnormal percentages were calculated for each group and for each SHIRPA response tested. Shaded boxes are SHIRPA responses with 50% or greater abnormal responses.

SHIRPA Response	Body position	Spontaneous activity	Respiratory rate	Touch escape	Transfer arousal	Gait	Piloerection	Visual placing	Trunk curl	Fear
WT Saline	8/0	8/0	8/0	8/0	7/1	8/0	8/0	8/0	7/1	8/0
Tg2576 Saline	6/2	6/2	8/0	5/3	6/2	8/0	8/0	6/2	5/3	3/5
WT VEEV TC-83	7/2	9/0	9/0	7/2	9/0	9/0	9/0	7/2	7/2	9/0
Tg2576 VEEV TC-83	2/6	1/7	7/1	1/7	0/8	8/0	8/0	4/4	2/6	0/8
Abnormal Percentage										
WT Saline	0%	0%	0%	0%	12.5%	0%	0%	0%	12.5%	0%
Tg2576 Saline	25%	25%	0%	37.5%	25%	0%	0%	25%	37.5%	62.5%
WT VEEV TC-83	22.2%	0%	0%	22%	0%	0%	0%	22.2%	22.2%	0%
Tg2576 VEEV TC-83	62.5%	87.5%	12.5%	87.5%	100%	0%	0%	50%	75%	100%

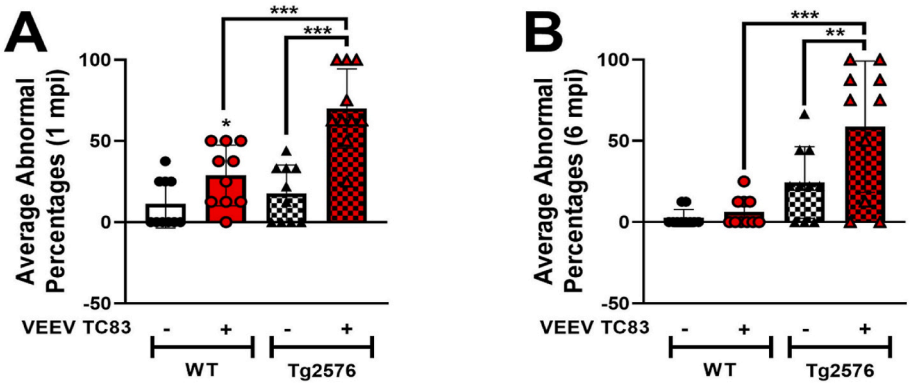

Fig. 2. VEEV TC-83 increases abnormal SHIRPA responses in Tg2576 at 1 and 6 mpi. The average percentages for each of the ten categories (represented by ten symbols per bar) were combined for each group (WT saline, WT VEEV TC-83, Tg2576 Saline, Tg2576 VEEV TC-83) at 1mpi (A) and 6 mpi (B). Statistical analyses were measured by a one-way ANOVA, Tukey's multiple comparison test, with a single pooled variance. Values are expressed as the mean ± SEM. *$p < 0.05$, **$p < 0.01$, ***$p < 0.001$.

TC-83 induced CNS inflammation in Tg2576 mice could play a role in perpetuating and exacerbating neurodegeneration and neurological sequelae.

Based on these observations and considering the role played by microglia and astrocytes in the inflammatory response, we investigated the expression and distribution of IBA1 (green) and GFAP (magenta) as markers of microglia and astrocytes, respectively (Fig. 5). Our focus was on the hippocampus, as it is one of the most affected areas in AD. Specifically, the DG (Fig. 5A1-A4), CA1 (Fig. 5B1-B4), and CA3 (Fig. 5C1-C4) were investigated. The extensive analysis of immunoreacted sections revealed significantly higher microglial activation in the overall hippocampus of WT VEEV TC-83 inoculated mice ($n = 5$) compared to WT saline mice ($n = 5$) and to Tg2576 VEEV TC-83 ($n = 5$) inoculated mice (*$p < 0.05$, **$p < 0.01$, Fig. 5G). Specifically, we observed significantly higher levels of IBA1 in DG and CA1 of WT VEEV TC-83 inoculated mice compared to WT saline (*$p < 0.05$, Fig. 5A1-A2, B1–B2, D, E) and an increasing trend in the WT mice inoculated with VEEV TC-83 compared to WT counterparts in the CA3 (Fig. 5C1-C2, F). We observed no significant differences between Tg2576 saline ($n = 5$) and Tg2576 VEEV TC-83 inoculated mice (Fig. 5D–G). Similarly, we observed a significant difference in astroglia activation in WT VEEV TC-83 mice compared to WT saline mice when the overall hippocampus was analyzed (*$p < 0.05$, Fig. 5K). Notably, the images and quantitative analyses show that the inoculation VEEV TC-83 induced significantly higher levels of GFAP in the DG of WT mice compared to WT saline (Fig. 5A1-A2, H) and an increasing trend in CA1 and CA3 (Fig. 5B1-B2, C1–C2, I, J). Also, no significant differences were observed within the Tg2576 mice groups in this case.

3.5. VEEV TC-83 inoculation induces neuropathological effects despite genotypes

To assess brain histopathology, groups of mice were euthanized 6 mpi, and brains were collected for histopathologic examination (Fig. 6); VEEV TC-83 inoculated brains from WT and Tg2576 mice served as controls (Fig. 6A–C, G-I). Standard paraffin sections were prepared and stained with H&E to assess encephalitis and meningitis. Encephalitis was evaluated in the cortex, striatum, brainstem, hippocampus, and cerebellum for perivascular mononuclear infiltrations (indicated as black arrows in Fig. 6D–J), microglial activation (elongated microglial nuclei labeled with white arrows in Fig. 6F–L) and microglial nodules (yellow circle in Fig. 6F–L). Similar areas from VEEV TC-83 inoculated brains do not show perivascular infiltrations (arrowhead in Fig. 6A–G) or microglial nodules (Fig. 6 C, I). An example of meningitis is demonstrated in Fig. 6E–K (black arrow) with perivascular mononuclear infiltrations within the subarachnoid space compared to the similar area of the VEEV TC-83 inoculated brain (no infiltration around a blood vessel in the subarachnoid space, arrowhead in Fig. 6B–H). Results of the evaluation (summarized in Supplemental Table 2) show inflammation in every VEEV TC-83 inoculated brain but none in saline inoculated ones. Inflammation is widely spread throughout all areas evaluated in WT and Tg2576 VEEV TC-83 inoculated groups. WT VEEV TC-83 inoculated mice show slightly wider areas with inflammation than Tg2576 VEEV TC-83 inoculated mice brains, but it's within the limits considering the sample variations.

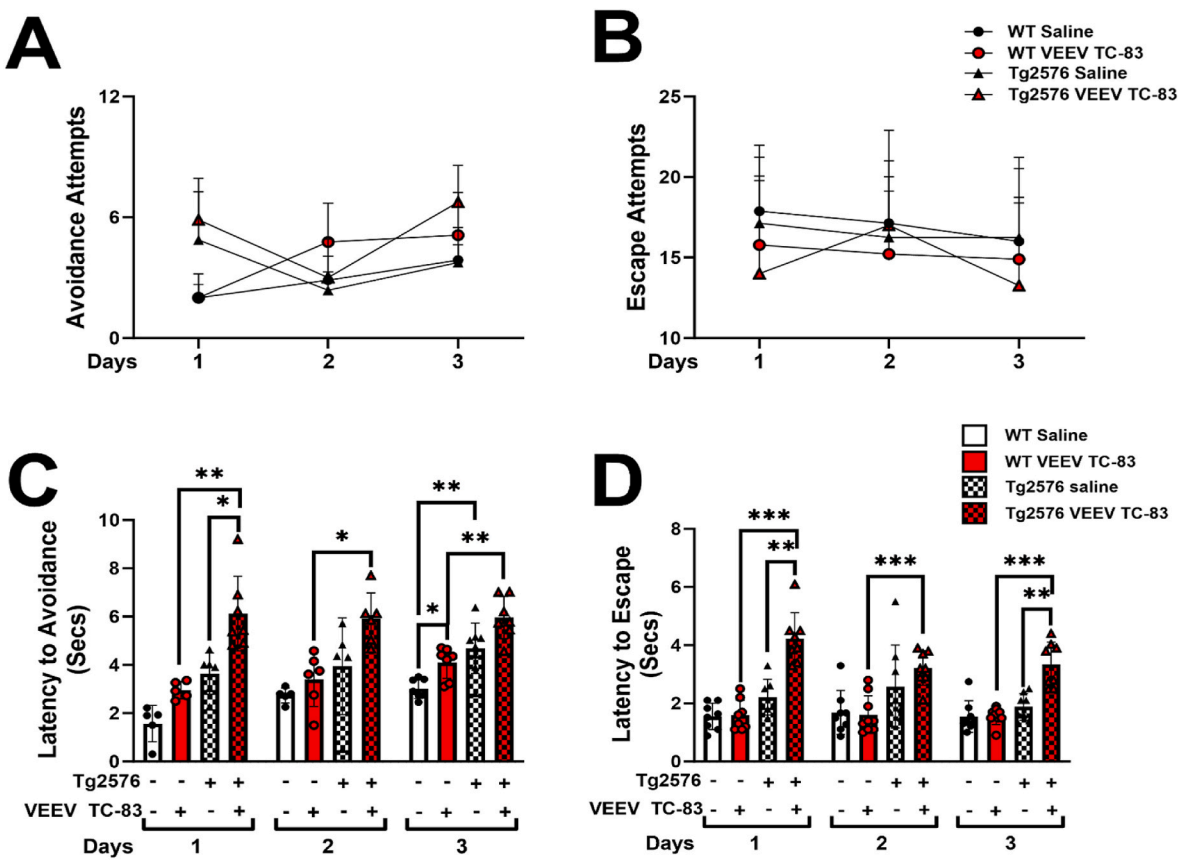

Fig. 3. VEEV TC83 inoculation impacts learning and memory. Active avoidance was performed at 6 mpi for three consecutive days, and the number of avoidance (A) and escape (B) attempts were recorded. The latency for the mice to avoid shock was recorded (C). The latency for the mice to escape shock was recorded for WT saline ($n = 8$), WT VEEV TC-83 ($n = 9$), Tg2576 saline ($n = 8$), Tg2576 VEEV TC-83 ($n = 8$) (D). Statistical analyses were measured by a mixed effects model with Geisser-Greenhouse correction, Tukey's multiple comparison test, with individual variances computed for each comparison. Values are expressed as the mean ± SEM. $*p < 0.05$, $**p < 0.01$, $***p < 0.001$.

3.6. *VEEV TC-83 increases expression, distribution, and measurement of amyloid beta in the mouse brain*

To investigate the effect of neurotropic VEEV TC-83 infection on Aβ generation and deposition, we employed two distinct approaches: an immunofluorescence analysis targeting Aβ plaques and a selective ELISA measuring Aβ peptides with C termini ending at residue 40 or 42. To specifically evaluate the influence of VEEV TC-83 infection on Aβ distribution and deposition in the hippocampus (DG [Fig. 7A1-A4]; CA1 [Fig. 7B1-B4]; CA3 [Fig. 7C1-C4]), we performed immunofluorescence experiments using an anti-Aβ antibody (Fig. 7A–C). The images and the quantitative analyses revealed no statistical differences among the WT saline ($n = 5$) or Tg2576 saline ($n = 5$) within DG (Fig. 7A1-A2 & D) or CA3 (Fig. 7C1-C2 & F) regions, but there was a significant increase in Aβ within the CA1 region ($**p < 0.01$, Fig. 7B1-B2 & E) and overall hippocampus ($**p < 0.01$, Fig. 7G). The levels of Aβ did not significantly increase following inoculation with VEEV TC-83, in either WT or Tg2576 mice in any specific brain region (Fig. 7) even though VEEV TC-83 inoculated mice showed an increasing trend of Aβ in all the areas considered (DG, CA1, CA3) (Fig. 7A–F) and in the overall hippocampus (Fig. 7G). When evaluating the overall hippocampus, there was a significant increase of Aβ levels compared between WT VEEV TC-83 and Tg2576 VEEV TC-83 ($*p < 0.05$, Fig. 7G). As expected, Tg2576 saline ($n = 5$) and Tg2576 VEEV TC-83 ($n = 5$) mice displayed higher Aβ levels than WT mice. Intriguingly, we did not find any Aβ plaques, most likely due to the young age of mice, but rather Aβ immunoreactivity was mostly localized intracellularly in the soma of pyramidal neurons in the CA1/CA3 regions, as well as in the hilus and granule cell layer of the DG.

ELISA analysis measurements demonstrate total Aβ1-40 as significantly higher in the brain extracts of Tg2576 saline mice ($n = 8$) compared to WT saline mice ($n = 8$; $*p < 0.05$, Fig. 7H) and when compared between WT VEEV TC-83 ($n = 9$) and Tg2576 VEEV TC-83 inoculated mice ($n = 8$; $*p < 0.05$, Fig. 7H). No differences were observed between WT and Tg2576 mice in the level of Aβ1-42 in either saline- or VEEV TC-83-inoculated groups (Fig. 7I). Furthermore, the Aβ1-42/1–40 ratio was quantified. The results exhibited a trend in the reduction of Aβ1-42/1–40 ratios in WT VEEV TC-83 vs WT saline; Tg2576 saline vs. WT saline; and in Tg2576 VEEV TC-83 vs Tg2576 saline (Fig. 7J). This represents a robust hallmark of Alzheimer's disease, establishing a significant association between Tg2576 mice and VEEV TC-83 infection.

4. Discussion

This study demonstrates that exposure to an alphavirus exacerbates the onset and development of neurodegenerative phenotypes and neuropathology associated with AD in WT and a preclinical mouse model of AD, Tg2576. While we observed modest changes in general health and signs of disease such as weight changes, overall, the mice did not display clinical outcomes related to VEEV infection during the acute phase, such as lethargy, reduced activity, development of discoordination, ataxia and/or paralysis. Compared to their saline controls, we measured the development of Aβ deposition, glial cell activation, neuroinflammation, and neuropathological characteristics coinciding with AD neuropathology following inoculation with VEEV TC-83 in WT and Tg2576 mice. Taken together, not only did we find that VEEV TC-83

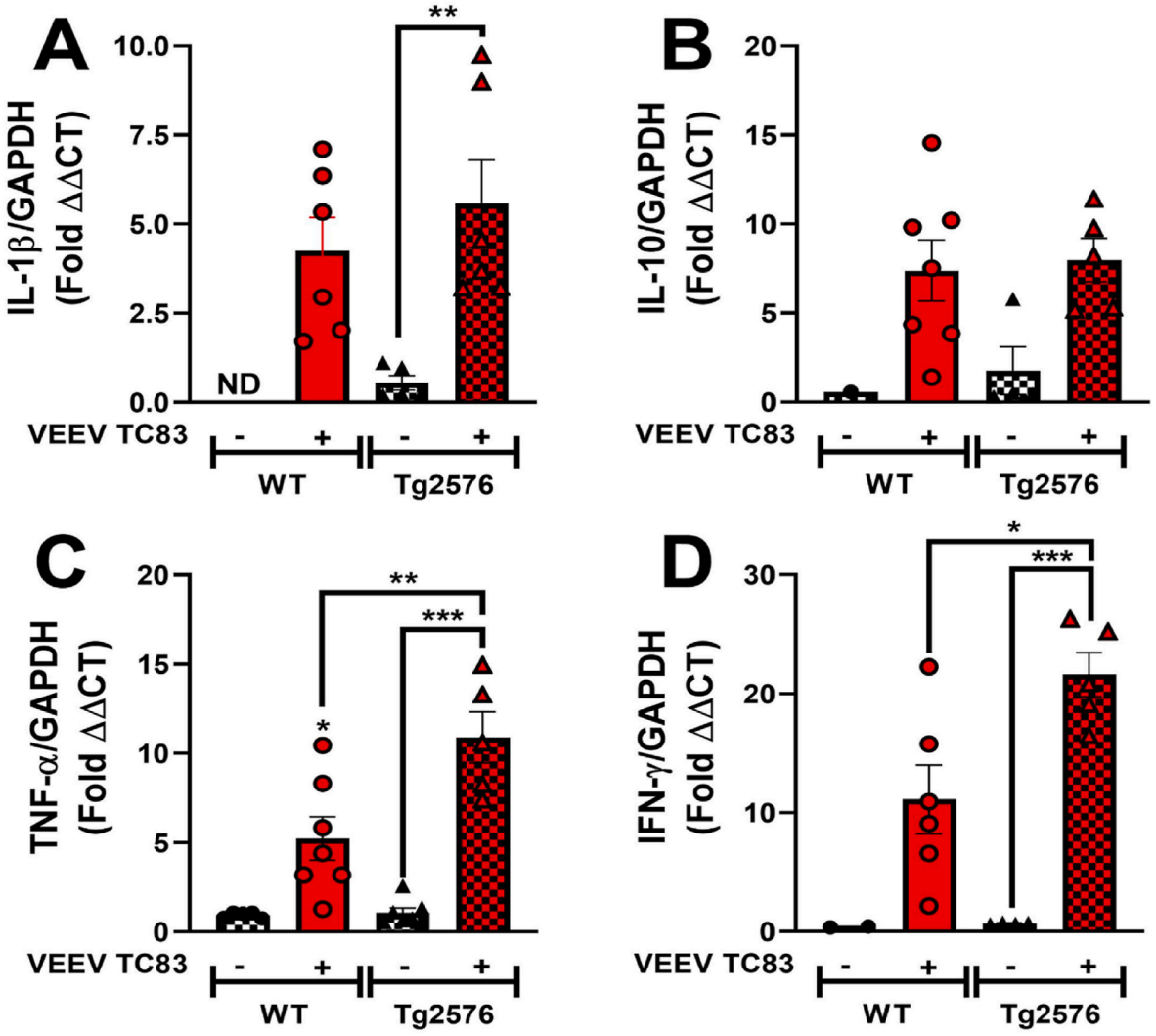

Fig. 4. CNS immune cytokine gene expression is modulated by VEEV TC-83. Total brain tissue homogenates collected 6 mpi were assayed from changes of expression in IL-1β (A), IL-10 (B), TNF-α (C), and IFN-γ (D) from WT saline ($n \leq 8$), WT VEEV TC-83 ($n \leq 9$), Tg2576 saline ($n \leq 8$), and Tg2576 VEEV TC-83 ($n \leq 8$). Statistical analyses were measured by ordinary one-way ANOVA followed by Tukey's multiple comparison test, with pooled variance. Values are expressed as the mean ± SEM. $^{*}p < 0.05$, $^{**}p < 0.01$, $^{***}p < 0.001$.

exposure in WT mice trigger the development of neuropathological outcomes related to AD, but that in a model genetically susceptible to developing AD, exposure to an encephalitic alphavirus exacerbates AD phenotypes.

VEEV infection characteristically induces an intense inflammatory response, initiating perivascular and interstitial mononuclear infiltrate in the brain. It induces neuropathology, including meningoencephalitis, gliosis, and multifocal neuropil vacuolation, which is localized to multiple regions, including the hippocampus (Charles et al., 2001; Kundin et al., 1966; Schoneboom et al., 2000; A. Taylor et al., 2015). Although VEEV TC-83, an attenuated strain of VEEV derived from the highly pathogenic Trinidad Donkey (TrD) strain, this virus can replicate and produce detectable titers in the brains of multiple mouse strains causing not lethal disease at low doses (Ludwig et al., 2001). In our studies all mice inoculated with VEEV TC-83 survived the acute phase as expected. We did not detect clinical symptoms in inoculated WT mice, as previously described (Ronca et al., 2017). However, we detected a significant increase in the weight loss percentage of inoculated Tg2576 mice compared to WT-inoculated mice during the acute stage of infection, which recovered over time. These preliminary observations coincide with post-alphavirus infection in humans, where symptoms begin to fade, and the illness resolves (Baxter and Heise, 2020). Despite recovery from clinical signs, or in asymptomatic cases of VEEV infection, approximately 4–14% of human survivors continue to develop neurological sequelae (Bowen et al., 1976; Carrera et al., 2013; Rivas et al., 1997; Ronca et al., 2016), which coincides with our observations.

Among the enduring neurological consequences experienced by VEEV survivors, symptoms such as paralysis, sensory impairments, headaches, fatigue, depression, seizures, neuropsychological alterations, and changes in mental status have been most frequently reported (Bowen et al., 1976; Carrera et al., 2013; Rivas et al., 1997). Furthermore, research on mice inoculated with encephalitic viruses has demonstrated significant hippocampal impairment and memory deficits, as evidenced by fear conditioning tests (Potter et al., 2015) and active avoidance experiments. Notably, abnormalities in hippocampal pathology have been linked to AD and other neurodegenerative disorders (Tombaugh et al., 2002). As a result, our study focused on assessing sensorimotor function, emotional reactivity, and aversive learning and memory using a modified SHIRPA assay and active avoidance tests. Active avoidance tests are particularly valuable for evaluating hippocampal-dependent cognitive functions (Anagnostaras et al., 2010; Chaudry et al., 2022; Kajs et al., 2022).

VEEV TC-83 inoculated WT and Tg2576 mice developed abnormal sensorimotor and emotional reactivity compared to saline control mice.

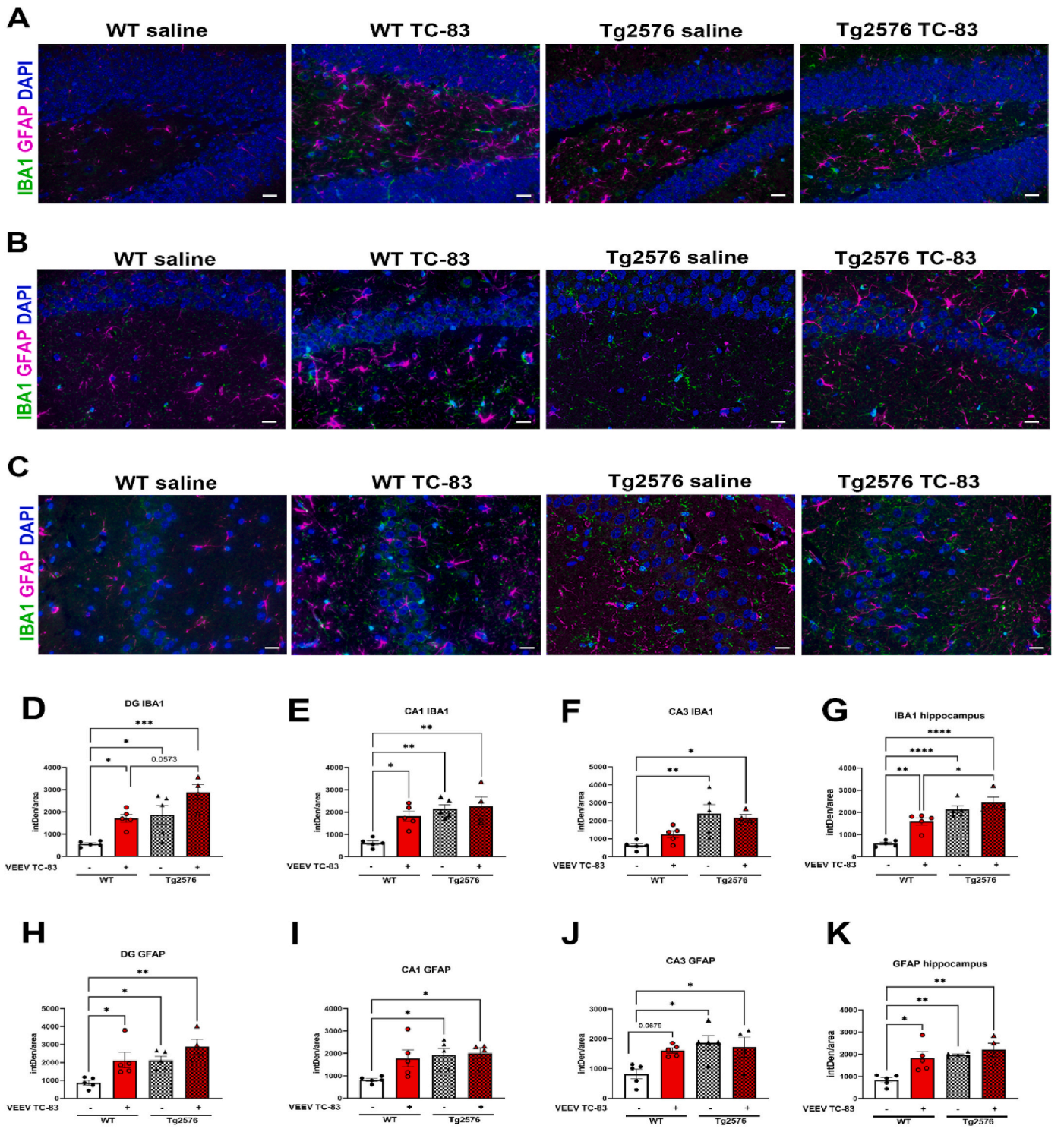

Fig. 5. Expression and distribution of IBA1 and GFAP in WT and Tg2576 mice inoculated with or without VEEV TC-83. Representative images of double immunofluorescence staining of IBA1 (green, microglia) and GFAP (magenta, astrocytes), DAPI (blue, nuclei) (A–C), and quantitative analyses (D–K). Hippocampal regions, DG (A1-A4), CA1 (B1–B4), and CA3 (C1–C4) were analyzed. Scale bar 20 μm. Statistical analyses were measured using a one-way ANOVA, followed by Tukey's multiple comparisons tests. Values are expressed as the mean ± SEM. WT saline ($n = 5$), WT VEEV TC-83 ($n = 5$), Tg2576 saline ($n = 5$), Tg2576 VEEV TC-83 ($n = 5$).

The neurological abnormalities detected in greater than half of WT mice inoculated with VEEV TC-83 were related to their neuropsychiatric state; however, those irregularities recovered at 6 mpi. In parallel, we observed more than half of Tg2576 mice inoculated with VEEV TC-83 developed neurological abnormalities, that unlike their WT counterparts, continued to stay elevated at 6 mpi. The abnormal behavioral outcomes were associated with motor behavior, reflex/sensory function, and neuropsychiatric states. We expected to detect similar responses in saline Tg2576 mice, in the absence of VEEV TC-83, since they develop age-associated deficits, and at this point in the study the mice were 9 months of age, but for the most part, all abnormal reactions were absent except for fear responses, which developed in greater than 50% of the Tg2576 saline mice. Fear in Tg2576 mice is a common observation made in this genotype (Dineley et al., 2002). Abnormalities in

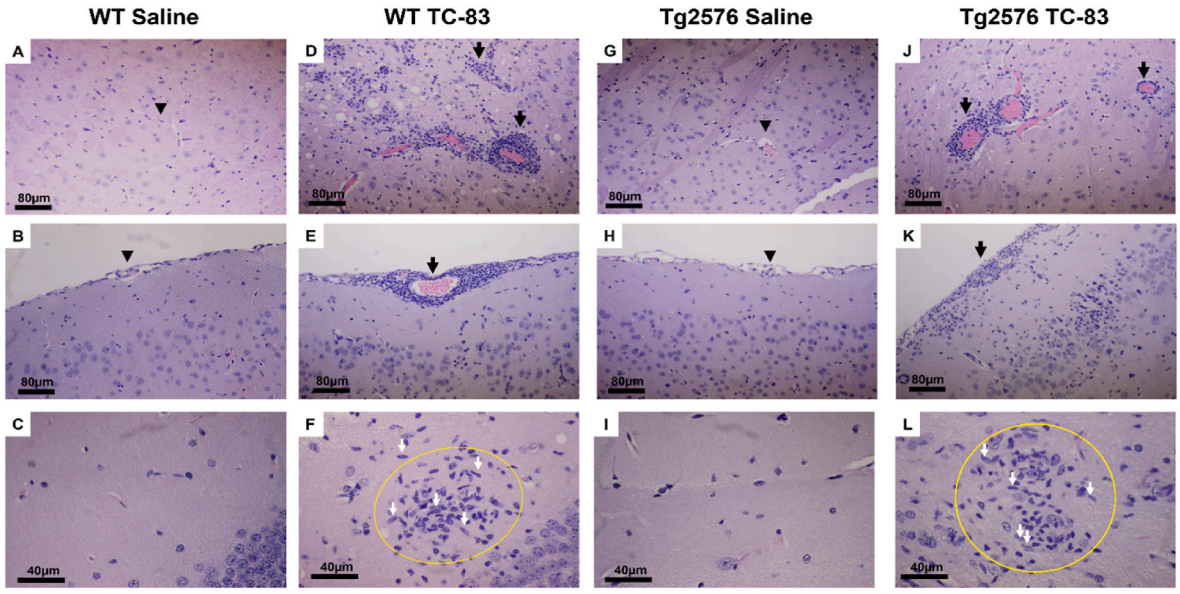

Fig. 6. Histopathological analysis of brains from WT ($n = 9$) and Tg2576 ($n = 8$) mice intranasally inoculated with VEEV TC-83. Brains of WT and Tg2576 mice were removed 6mpi for histopathologic examination. WT saline ($n = 8$) and Tg2576 saline ($n = 8$) mice served as controls (6 A-C, G-I). Standard paraffin sections were prepared and stained H&E to assess encephalitis and meningitis. Encephalitis was evaluated in the cortex, striatum, brainstem, hippocampus, and cerebellum for perivascular mononuclear infiltrations (black arrows in 6D, J), microglial activation (elongated microglial nuclei labeled with white arrows in 6 F, L) and microglial nodules (yellow circle in 6 F, L). Similar areas from uninfected brains do not show perivascular infiltrations (arrowhead in 6 A, J) or microglial nodules (6C, I). Scale bar = 80 μm for A, B, D, E, G, H, J, and K; Scale bar = 40 μm for C, F, I, and L.

neuropsychiatric states were common among the VEEV TC-83 inoculated WT and Tg2576 mice and were exaggerated responses to the normal, indicating anxiety-like behavior, irritability, or dementia, which are associated with the sequelae of alphaviruses (Reisberg et al., 1987) and with AD (Cerejeira et al., 2012). Moreover, neuropsychiatric symptoms, alongside behavioral disorders, deficits in locomotor activity, and changes in reflex and sensory function, precede cognitive deficits in AD (Albers et al., 2015; Buchman and Bennett, 2011; Cortes et al., 2018). Observations related to these outcomes including abnormal motor behavior, with an overactive and irritable body position, abnormal gait, a hyperactive trunk curl, vigorous extension during visual placing, extremely excited transfer arousal, vigorous attempts to escape touch, and hyperactive fear responses were inflated only in VEEV TC-83 inoculated Tg2576 mice, suggesting that within the AD phenotype, encephalitic infections aggravate AD pathogenesis. These abnormal responses triggered further behavioral studies in quantifiable learning and memory assays via active avoidance. Previous studies demonstrate that in animal models of neurodegenerative disorders, such as AD, cognitive function and learning and memory are significantly impaired (Anagnostaras et al., 2010; Chaudry et al., 2022; Kajs et al., 2022; Webster et al., 2014) and that VEEV infections can have an adverse effect on learning memory (Dave and Klein, 2023; Ronca et al., 2016). Thus, we expected that VEEV TC-83 inoculated mice, regardless of genotype, would not only develop altered learning and memory outcomes, but those VEEV TC-83 inoculated Tg2576 mice would have impaired learning and memory responses, measured by reduced attempts to avoid or escape shock during aversive fear conditioning. Surprisingly, we found that infection did not alter the number of times that either WT or Tg2576 mice avoided or escaped shock during active avoidance. However, we found that VEEV TC-83 inoculation in both WT and Tg2576 mice increased the amount of time it took to avoid or escape shock, thus increasing latency. Even more interesting is that only VEEV TC-83 inoculated Tg2576 mice significantly increased their latency to avoid shock that increased over trial days. These measurements indicate that exposure to VEEV TC-83 in a model predisposed to develop AD exacerbates the decline in cognition, heightening fear, anxiety, and caution; similar outcomes are observed in patients developing AD (Zhou et al., 2022; Zielinski et al., 1993).

Based on behavioral outcomes, VEEV TC-83 impacts the CNS regardless of the genetic background of the experimental model and behavioral deficits, justifying further studies into the neuropathology and neuroimmunology induced by VEEV TC-83. Neuroinflammation is a common hallmark for both AD and CNS infections (Cle et al., 2020). In AD and CNS infections, pro- and anti-inflammatory signaling is primarily initiated by CNS resident immune cells, the astrocytes, and microglia (Di Benedetto et al., 2022; Russo and McGavern, 2015). Neuroinflammation is also linked to neurodegeneration and neuronal loss, which are features that coincidently are associated with amyloid plaque formation (DeTure and Dickson, 2019; Kinney et al., 2018; Sung et al., 2020). In this study, intranasal VEEV TC-83 inoculation increased total CNS localized immune cytokines in WT and Tg2576 mice. Previous studies found that the VEEV TC-83 strain of VEEV induces robust inflammation during the early stages of disease progression in the brain of hamsters (Jahrling et al., 1976). This infection can lead to the activation of microglial cells, which mediate neuron communication through the production of proinflammatory factors such as cytokines including IL-1β, IL-10, TNF-α, and IFN-γ ultimately facilitating the migration of immune cells across the blood-brain barrier (BBB) (Ramesh et al., 2013). These alterations in cytokine expression can increase the permeability of the BBB and play a crucial role in activating several signaling pathways located in different brain cells (Carrano et al., 2012). This cascade of events may result in hyperexcitability of the neuronal network, which is important in the pathophysiology of AD (Clarkson et al., 2017; Targa Dias Anastacio, Matosin and Ooi, 2022). Our analysis indicates that VEEV TC-83 inoculation results in the production of immunoregulatory molecules, including IL-1β, IL-10, TNF-α, and IFN-γ, which are implicated in neurodegenerative processes (Keck et al., 2018; Keck et al., 2018b; Sharma and Knollmann-Ritschel, 2019). Cellular and molecular mechanisms resulting from injury or infections, underlying the development of proinflammatory cytokines and chemokines in the CNS, are canonically triggered and modulated by astrocytes and microglia (Hanisch, 2002; Murphy et al., 1997), which contribute to the impairment of memory function (Gaudio et al., 2015). Given the importance of the hippocampus in learning and memory and AD

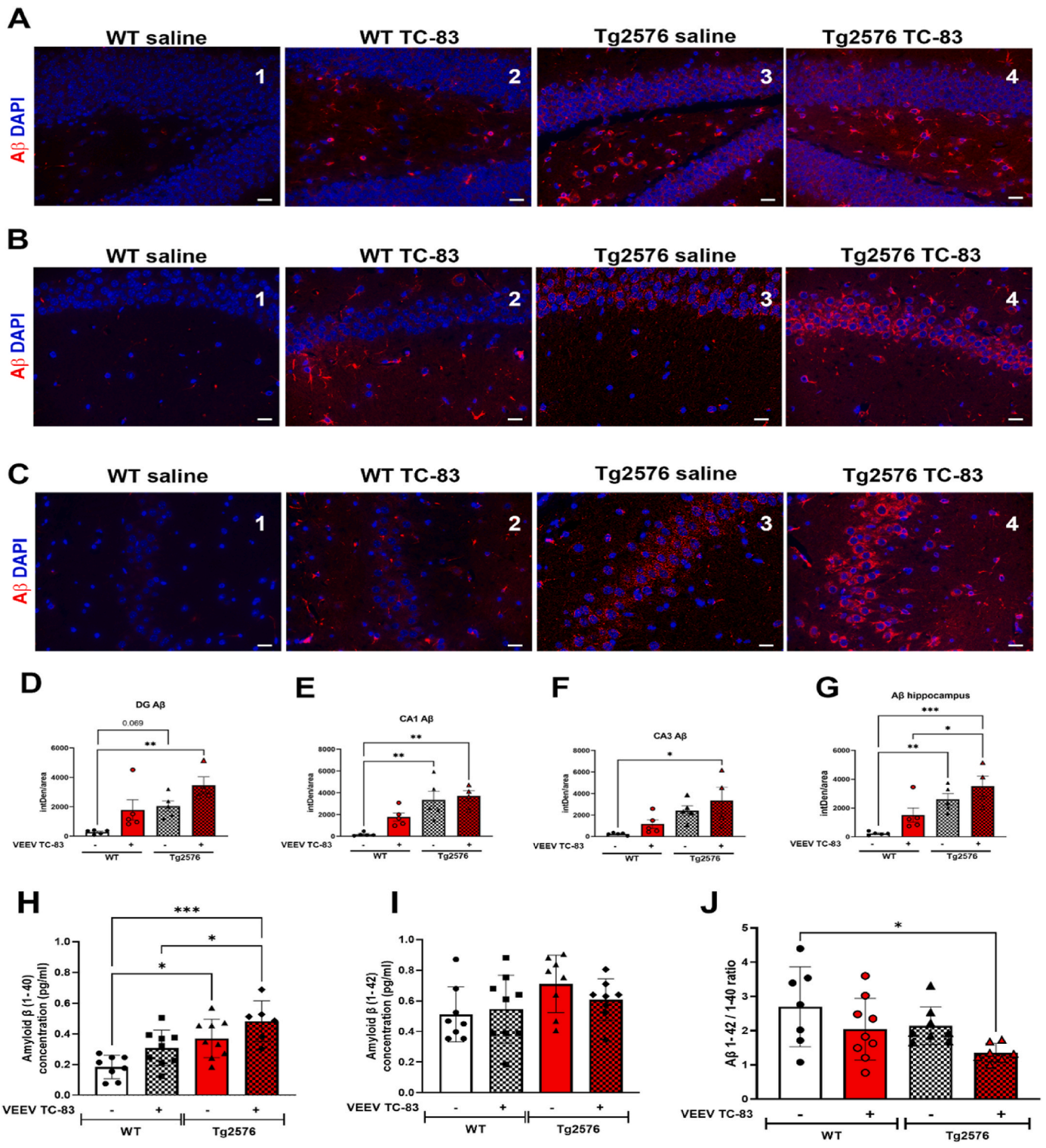

Fig. 7. VEEV TC-83-induced expression and distribution of Aβ in WT and Tg2576 mice. Representative images of immunofluorescence staining of Aβ (red), DAPI (blue, nucleus), and quantitative analyses of Ab in the DG (A1-A4 & D), CA1 (B1–B4 & E), and CA3 (C1–C4 & F) and overall hippocampus (G). Scale bar 20 μm. Statistical analyses were measured using a one-way ANOVA, following Tukey's multiple comparisons test. Values are expressed as the mean ± SEM. Measurement of Aβ1-40 (H), Aβ1-42 (I), and the ratio of Aβ 1–42/1-40 (J) was measured in total brain homogenates. Statistical analyses were measured using an ordinary two-way ANOVA, following Tukey's multiple comparisons test. Values are expressed as the mean ± SEM. *$p < 0.05$, **$p < 0.01$, ***$p < 0.001$. WT saline ($n = 5$-8), WT VEEV TC-83 ($n = 5$-9), Tg2576 saline ($n = 5$-8), Tg2576 VEEV TC-83 ($n = 5$-8).

neuropathogenesis (Tombaugh et al., 2002), we found increased activation of hippocampal astrocytes and microglia in VEEV TC-83 inoculated mice, regardless of genotype, which is well characterized to lead to encephalitis and neurological damage (Cain et al., 2017; Sharma et al., 2011). In parallel, we identified neuropathological changes related to neuroinflammation in the hippocampus. We measured increased microglial activation in the hippocampi of all VEEV TC-83 inoculated mice and found activated microglia, but not astrocytes, to be

significantly increased in VEEV TC-83 inoculated Tg2576 mice compared to VEEV TC-83 inoculated WT mice. However, no differences were detected in VEEV TC-83 inoculated Tg2576 mice. Nevertheless, significant disparities were evident between genotypes, consistent with expectations given that Tg2576 mice typically manifest gliosis by 6 months of age, coinciding with the 9-month age range of the animals in our study. The absence of discernible distinctions in inoculated Tg2576 mice implies that gliosis may reach a saturation point following inoculation with VEEV TC-83. Despite the lack of notable variances in GFAP and Iba1 expression, the observed neuroinflammatory alterations and exacerbated behavioral changes in Tg2576 mice inoculated with VEEV TC-83 compared to their WT counterparts, suggest an exacerbation of AD-related pathology induced by VEEV inoculation. Furthermore, analysis of brain histopathology showed that encephalitis was characterized by perivascular mononuclear infiltrations, microglial activation, and microglial nodules in the cortex, striatum, brainstem, hippocampus, and cerebellum. Although saline inoculated Tg2576 mice developed neuroinflammatory characteristics, VEEV TC-83 inoculated Tg2576 mice displayed an increased neuroinflammatory phenotype compared to their inoculated controls, including increased perivascular cuffing and GFAP and Iba1 staining. Glia, microglia, and astrocyte activations are associated with cerebral amyloid deposits necessary for phagocytic activity induction (D'Andrea et al., 2004).

A preclinical study of AD shows sex differences in AD development. The female Tg-F344-AD rats have higher levels of Aβ peptides, amyloid plaques, and microgliosis in the hippocampus than male rats and were shown to enhance learning and memory by stimulating GluA2 trafficking, which may provide a neuroprotective function in hippocampal with improved spatial learning in Tg-AD females (Chaudry et al., 2022). The prefrontal cortex is involved in processing anxiety, which can interfere with goal-directed behavior and cognitive performance (Park and Moghaddam, 2017). Previous studies of the hippocampus are critical to cognition and variables influencing learning and memory processes (Danilewicz et al., 1992). In this study, we used VEEV TC-83 to target learning and memory, which resulted in delayed response latencies reflecting caution and indicating significant loss of spatial ability and memory dysfunction. In preclinical AD, mouse models that contain a mutation in amyloid precursor protein (APP) have been widely used as models of AD, which play an essential role in cognitive function (Webster et al., 2014). A recent study in transgenic animal models of AD has shown that disrupting neurogenesis and neural progenitor cell homeostasis in the hippocampus causes learning and memory impairments, developing into an early onset AD (Haughey et al., 2002). Considering our findings, the VEEV TC-83 inoculated mice took longer to avoid the shock, supporting spatial memory and recognition. Although additional studies are warranted, expanding on the use of AD preclinical models and additional ages, our data supports the notion that exposure to encephalitic viruses do trigger the progression of AD neuropathology, thus supporting the infectious etiology hypothesis of AD.

A recent report utilizing information from national biobanks suggests that exposure to common viral pathogens increases the risk of developing Alzheimer's and other neurodegenerative diseases (Blackhurst and Funk, 2023). Several studies have shown that viral infections, such as Herpes simplex encephalitis, Epstein-Barr virus, Eastern Equine Encephalitis virus (EEEV), Western Equine Encephalitis virus (WEEV), and Venezuelan Equine Encephalitis Virus (VEEV), correlate with negative neurological consequences even after the acute phase, suggesting a potential role in developing and progressing neurodegenerative disorders, particularly AD (Bantle et al., 2019; Piekut et al., 2022; Ronca et al., 2017). In our study, we observed the neuropathology associated with VEEV infections and its potential correlation to the deposition of Aβ in the brain. Our study observed a remarkable reduction in the Aβ1-42/1–40 ratio in the brains of Tg2576 mice inoculated with VEEV TC-83 compared to WT saline and WT VEEV TC-83 inoculated mice. These findings align with the inverse relationship between plasma Aβ1-42/1–40 and cortical Aβ burden observed in AD patients (Rembach et al., 2014). Furthermore, our hippocampal immunofluorescent staining, using microglia marker Iba-1 and astrocyte marker GFAP, indicates that VEEV TC-83 is associated with the activation of astrocytes and microglia in the CNS, possibly leading to increased neuroinflammation.

5. Conclusion

Despite evidence and surmounting research on amyloid-induced pathways of AD, the mechanisms underlying amyloid beta deposition are not fully identified. Several neurotropic pathogens are associated with developing AD pathogenesis, and the antimicrobial properties of amyloid-beta peptides support the hypothesis that pathogens, including viruses, increase the risk for amyloid-beta plaque formation. Our findings further support that exposure to encephalitic viruses, such as VEEV TC-83, may trigger the onset and severity of AD pathogenesis using a model that predisposed to develop AD. Based on our data, and previous reports, neuroinflammatory responses long after infection has cleared the brain, support the infectious etiology hypothesis of AD **(Schematic 2)**.

Funding sources

This research was supported by the National Institutes of Health (NIH), National Institute on Aging (NIA), United States R56AG079190 to I.E.C.. S.P. was supported by John S. Dunn Endowment.

CRediT authorship contribution statement

Chanida Fongsaran: Writing – review & editing, Writing – original draft, Visualization, Validation, Software, Resources, Project administration, Methodology, Investigation, Formal analysis, Data curation, Conceptualization. **Krit Jirakanwisal:** Writing – review & editing, Methodology. **Bi-Hung Peng:** Visualization, Validation, Formal analysis. **Anna Fracassi:** Visualization, Validation, Formal analysis. **Giulio Taglialatela:** Writing – review & editing, Validation. **Kelly T. Dineley:** Writing – review & editing. **Slobodan Paessler:** Writing – review & editing, Supervision. **Irma E. Cisneros:** Writing – review & editing, Supervision, Resources, Project administration, Investigation, Funding acquisition, Formal analysis, Conceptualization.

Declaration of competing interest

The authors declare that they have no known competing financial interests or personal relationships that could have appeared to influence the work reported in this paper.

Data availability

Data will be made available on request.

Acknowledgements

We would like to thank Neuroinfectious Disease Initiative at UTMB for technical assistance with this project.

Appendix A. Supplementary data

Supplementary data to this article can be found online at https://doi.org/10.1016/j.bbih.2024.100780.

References

Aguilar, P.V., Estrada-Franco, J.G., Navarro-Lopez, R., Ferro, C., Haddow, A.D., Weaver, S.C., 2011. Endemic Venezuelan equine encephalitis in the Americas:

hidden under the dengue umbrella. Future Virol. 6 (6), 721–740. https://doi.org/10.2217/FVL.11.5.
Albers, M.W., Gilmore, G.C., Kaye, J., Murphy, C., Wingfield, A., Bennett, D.A., Zhang, L. I., 2015. At the interface of sensory and motor dysfunctions and Alzheimer's disease. Alzheimers Dement 11 (1), 70–98. https://doi.org/10.1016/j.jalz.2014.04.514.
Anagnostaras, S.G., Wood, S.C., Shuman, T., Cai, D.J., Leduc, A.D., Zurn, K.R., Herrera, G.M., 2010. Automated assessment of pavlovian conditioned freezing and shock reactivity in mice using the video freeze system. Front. Behav. Neurosci. 4 https://doi.org/10.3389/fnbeh.2010.00158.
Bantle, C.M., Phillips, A.T., Smeyne, R.J., Rocha, S.M., Olson, K.E., Tjalkens, R.B., 2019. Infection with mosquito-borne alphavirus induces selective loss of dopaminergic neurons, neuroinflammation and widespread protein aggregation. NPJ Parkinsons Dis 5, 20. https://doi.org/10.1038/s41531-019-0090-8.
Baxter, V.K., Heise, M.T., 2020. Immunopathogenesis of alphaviruses. Adv. Virus Res. 107, 315–382. https://doi.org/10.1016/bs.aivir.2020.06.002.
Blackhurst, B.M., Funk, K.E., 2023. Viral pathogens increase risk of neurodegenerative disease. Nat. Rev. Neurol. 19 (5), 259–260. https://doi.org/10.1038/s41582-023-00790-6.
Bocan, T.M., Stafford, R.G., Brown, J.L., Akuoku Frimpong, J., Basuli, F., Hollidge, B.S., Smith, D.R., 2019. Characterization of brain inflammation, apoptosis, hypoxia, blood-brain barrier integrity and metabolism in Venezuelan equine encephalitis virus (VEEV TC-83) exposed mice by in vivo positron emission tomography imaging. Viruses 11 (11). https://doi.org/10.3390/v11111052.
Bowen, G.S., Fashinell, T.R., Dean, P.B., Gregg, M.B., 1976. Clinical aspects of human Venezuelan equine encephalitis in Texas. Bull. Pan Am. Health Organ. 10 (1), 46–57.
Buchman, A.S., Bennett, D.A., 2011. Loss of motor function in preclinical Alzheimer's disease. Expert Rev. Neurother. 11 (5), 665–676. https://doi.org/10.1586/ern.11.57.
Cain, M.D., Salimi, H., Gong, Y., Yang, L., Hamilton, S.L., Heffernan, J.R., Klein, R.S., 2017. Virus entry and replication in the brain precedes blood-brain barrier disruption during intranasal alphavirus infection. J. Neuroimmunol. 308, 118–130. https://doi.org/10.1016/j.jneuroim.2017.04.008.
Carrano, A., Hoozemans, J.J., van der Vies, S.M., van Horssen, J., de Vries, H.E., Rozemuller, A.J., 2012. Neuroinflammation and blood-brain barrier changes in capillary amyloid angiopathy. Neurodegener. Dis. 10 (1–4), 329–331. https://doi.org/10.1159/000334916.
Carrera, J.P., Forrester, N., Wang, E., Vittor, A.Y., Haddow, A.D., López-Vergès, S., Weaver, S.C., 2013. Eastern equine encephalitis in Latin America. N. Engl. J. Med. 369 (8), 732–744. https://doi.org/10.1056/NEJMoa1212628.
Cerejeira, J., Lagarto, L., Mukaetova-Ladinska, E.B., 2012. Behavioral and psychological symptoms of dementia. Front. Neurol. 3, 73. https://doi.org/10.3389/fneur.2012.00073.
Charles, P.C., Trgovcich, J., Davis, N.L., Johnston, R.E., 2001. Immunopathogenesis and immune modulation of Venezuelan equine encephalitis virus-induced disease in the mouse. Virology 284 (2), 190–202. https://doi.org/10.1006/viro.2001.0878.
Chaudry, O., Ndukwe, K., Xie, L., Figueiredo-Pereira, M., Serrano, P., Rockwell, P., 2022. Females exhibit higher GluA2 levels and outperform males in active place avoidance despite increased amyloid plaques in TgF344-Alzheimer's rats. Sci. Rep. 12 (1), 19129 https://doi.org/10.1038/s41598-022-23801-w.
Clarkson, B.D.S., Kahoud, R.J., McCarthy, C.B., Howe, C.L., 2017. Inflammatory cytokine-induced changes in neural network activity measured by waveform analysis of high-content calcium imaging in murine cortical neurons. Sci. Rep. 7 (1), 9037. https://doi.org/10.1038/s41598-017-09182-5.
Cle, M., Eldin, P., Briant, L., Lannuzel, A., Simonin, Y., Van de Perre, P., Salinas, S., 2020. Neurocognitive impacts of arbovirus infections. J. Neuroinflammation 17 (1), 233. https://doi.org/10.1186/s12974-020-01904-3.
Cortes, N., Andrade, V., Maccioni, R.B., 2018. Behavioral and neuropsychiatric disorders in Alzheimer's disease. J. Alzheimers Dis. 63 (3), 899–910. https://doi.org/10.3233/JAD-180005.
D'Andrea, M.R., Cole, G.M., Ard, M.D., 2004. The microglial phagocytic role with specific plaque types in the Alzheimer disease brain. Neurobiol. Aging 25 (5), 675–683. https://doi.org/10.1016/j.neurobiolaging.2003.12.026.
Danilewicz, M., Sikorska, B., Wagrowska-Danilewicz, M., 1992. [Endometriosis of the large intestine]. Pol. Tyg. Lek. 47 (29–30), 651–652.
Dave, V.A., Klein, R.S., 2023. The multitaskers of the brain: glial responses to viral infections and associated post-infectious neurologic sequelae. Glia 71 (4), 803–818. https://doi.org/10.1002/glia.24294.
DeTure, M.A., Dickson, D.W., 2019. The neuropathological diagnosis of Alzheimer's disease. Mol. Neurodegener. 14 (1), 32. https://doi.org/10.1186/s13024-019-0333-5.
Di Benedetto, G., Burgaletto, C., Bellanca, C.M., Munafò, A., Bernardini, R., Cantarella, G., 2022. Role of microglia and astrocytes in Alzheimer's disease: from neuroinflammation to Ca. Cells 11 (17). https://doi.org/10.3390/cells11172728.
Diehl, M.M., Bravo-Rivera, C., Quirk, G.J., 2019. The study of active avoidance: a platform for discussion. Neurosci. Biobehav. Rev. 107, 229–237. https://doi.org/10.1016/j.neubiorev.2019.09.010.
Dineley, K.T., Xia, X., Bui, D., Sweatt, J.D., Zheng, H., 2002. Accelerated plaque accumulation, associative learning deficits, and up-regulation of alpha 7 nicotinic receptor protein in transgenic mice co-expressing mutant human presenilin 1 and amyloid precursor proteins. J. Biol. Chem. 277 (25), 22768–22780. https://doi.org/10.1074/jbc.M200164200.
Ehrenkranz, N.J., Ventura, A.K., 1974. Venezuelan equine encephalitis virus infection in man. Annu. Rev. Med. 25, 9–14. https://doi.org/10.1146/annurev.me.25.020174.000301.
Fracassi, A., Marcatti, M., Tumurbaatar, B., Woltjer, R., Moreno, S., Taglialatela, G., 2023. TREM2-induced activation of microglia contributes to synaptic integrity in cognitively intact aged individuals with Alzheimer's neuropathology. Brain Pathol. 33 (1), e13108 https://doi.org/10.1111/bpa.13108.
Gardner, C.L., Burke, C.W., Tesfay, M.Z., Glass, P.J., Klimstra, W.B., Ryman, K.D., 2008. Eastern and Venezuelan equine encephalitis viruses differ in their ability to infect dendritic cells and macrophages: impact of altered cell tropism on pathogenesis. J. Virol. 82 (21), 10634–10646. https://doi.org/10.1128/JVI.01323-08.
Gaudio, A., Muratore, F., Fiore, V., Rapisarda, R., Signorelli, S.S., Fiore, C.E., 2015. Decreased bone cortical density at the forearm in subjects with subclinical peripheral arterial disease. Osteoporos. Int. 26 (6), 1747–1753. https://doi.org/10.1007/s00198-015-3057-6.
Geschwind, M.D., Haman, A., Miller, B.L., 2007. Rapidly progressive dementia. Neurol. Clin. 25 (3), 783–807. https://doi.org/10.1016/j.ncl.2007.04.001 vii.
Gleiser, C.A., Gochenour Jr., W.S., Berge, T.O., Tigertt, W.D., 1962. The comparative pathology of experimental Venezuelan equine encephalomyelitis infection in different animal hosts. J. Infect. Dis. 110, 80–97. https://doi.org/10.1093/infdis/110.1.80.
Hanisch, U.K., 2002. Microglia as a source and target of cytokines. Glia 40 (2), 140–155. https://doi.org/10.1002/glia.10161.
Haughey, N.J., Nath, A., Chan, S.L., Borchard, A.C., Rao, M.S., Mattson, M.P., 2002. Disruption of neurogenesis by amyloid beta-peptide, and perturbed neural progenitor cell homeostasis, in models of Alzheimer's disease. J. Neurochem. 83 (6), 1509–1524. https://doi.org/10.1046/j.1471-4159.2002.01267.x.
Jahrling, P.B., Navarro, E., Scherer, W.F., 1976. Interferon induction and sensitivity as correlates to virulence of Venezuelan encephalitis viruses for hamsters. Arch. Virol. 51 (1–2), 23–35. https://doi.org/10.1007/BF01317831.
Julander, J.G., Skirpstunas, R., Siddharthan, V., Shafer, K., Hoopes, J.D., Smee, D.F., Morrey, J.D., 2008. C3H/HeN mouse model for the evaluation of antiviral agents for the treatment of Venezuelan equine encephalitis virus infection. Antivir. Res. 78 (3), 230–241. https://doi.org/10.1016/j.antiviral.2008.01.007.
Kajs, B.L., Loewke, A.C., Dorsch, J.M., Vinson, L.T., Gunaydin, L.A., 2022. Divergent encoding of active avoidance behavior in corticostriatal and corticolimbic projections. Sci. Rep. 12 (1), 10731 https://doi.org/10.1038/s41598-022-14930-3.
Keck, F., Khan, D., Roberts, B., Agrawal, N., Bhalla, N., Narayanan, A., 2018a. Mitochondrial-directed antioxidant reduces microglial-induced inflammation in murine in vitro model of TC-83 infection. Viruses 10 (11). https://doi.org/10.3390/v10110606.
Keck, F., Kortchak, S., Bakovic, A., Roberts, B., Agrawal, N., Narayanan, A., 2018b. Direct and indirect pro-inflammatory cytokine response resulting from TC-83 infection of glial cells. Virulence 9 (1), 1403–1421. https://doi.org/10.1080/21505594.2018.1509668.
Kinney, J.W., Bemiller, S.M., Murtishaw, A.S., Leisgang, A.M., Salazar, A.M., Lamb, B.T., 2018. Inflammation as a central mechanism in Alzheimer's disease. Alzheimers Dement (N Y) 4, 575–590. https://doi.org/10.1016/j.trci.2018.06.014.
Kundin, W.D., Liu, C., Rodina, P., 1966. Pathogenesis of Venezuelan equine encephalomyelitis virus. I. Infection in suckling mice. J. Immunol. 96 (1), 39–48.
Lalonde, R., Filali, M., Strazielle, C., 2021. SHIRPA as a neurological screening battery in mice. Curr. Protoc. 1 (5), e135 https://doi.org/10.1002/cpz1.135.
Ludwig, G.V., Turell, M.J., Vogel, P., Kondig, J.P., Kell, W.K., Smith, J.F., Pratt, W.D., 2001. Comparative neurovirulence of attenuated and non-attenuated strains of Venezuelan equine encephalitis virus in mice. Am. J. Trop. Med. Hyg. 64 (1–2), 49–55. https://doi.org/10.4269/ajtmh.2001.64.49.
Mulder, D.W., Parrott, M., Thaler, M., 1951. Sequelae of western equine encephalitis. Neurology 1 (4), 318–327. https://doi.org/10.1212/wnl.1.7-8.318.
Murphy, M., Dutton, R., Koblar, S., Cheema, S., Bartlett, P., 1997. Cytokines which signal through the LIF receptor and their actions in the nervous system. Prog. Neurobiol. 52 (5), 355–378. https://doi.org/10.1016/s0301-0082(97)00020-8.
Nelson, P.T., Alafuzoff, I., Bigio, E.H., Bouras, C., Braak, H., Cairns, N.J., Beach, T.G., 2012. Correlation of Alzheimer disease neuropathologic changes with cognitive status: a review of the literature. J. Neuropathol. Exp. Neurol. 71 (5), 362–381. https://doi.org/10.1097/NEN.0b013e31825018f7.
Onisiforou, A., Spyrou, G.M., 2021. Identification of viral-mediated pathogenic mechanisms in neurodegenerative diseases using network-based approaches. Briefings Bioinf. 22 (6) https://doi.org/10.1093/bib/bbab141.
Paessler, S., Rijnbrand, R., Stein, D.A., Ni, H., Yun, N.E., Dziuba, N., Zacks, M.A., 2008. Inhibition of alphavirus infection in cell culture and in mice with antisense morpholino oligomers. Virology 376 (2), 357–370. https://doi.org/10.1016/j.virol.2008.03.032.
Park, J., Moghaddam, B., 2017. Impact of anxiety on prefrontal cortex encoding of cognitive flexibility. Neuroscience 345, 193–202. https://doi.org/10.1016/j.neuroscience.2016.06.013.
Peiris, J.S., Amerasinghe, P.H., Amerasinghe, F.P., Calisher, C.H., Perera, L.P., Arunagiri, C.K., Karunaratne, S.H., 1994. Viruses isolated from mosquitoes collected in Sri Lanka. Am. J. Trop. Med. Hyg. 51 (2), 154–161. https://doi.org/10.4269/ajtmh.1994.51.154.
Piekut, T., Hurła, M., Banaszek, N., Szejn, P., Dorszewska, J., Kozubski, W., Prendecki, M., 2022. Infectious agents and Alzheimer's disease. J. Integr. Neurosci. 21 (2), 73. https://doi.org/10.31083/j.jin2102073.
Potter, M.C., Baxter, V.K., Mathey, R.W., Alt, J., Rojas, C., Griffin, D.E., Slusher, B.S., 2015. Neurological sequelae induced by alphavirus infection of the CNS are attenuated by treatment with the glutamine antagonist 6-diazo-5-oxo-l-norleucine. J. Neurovirol. 21 (2), 159–173. https://doi.org/10.1007/s13365-015-0314-6.
Ramesh, G., MacLean, A.G., Philipp, M.T., 2013. Cytokines and chemokines at the crossroads of neuroinflammation, neurodegeneration, and neuropathic pain. Mediat. Inflamm. 2013, 480739 https://doi.org/10.1155/2013/480739.

Reisberg, B., Borenstein, J., Salob, S.P., Ferris, S.H., Franssen, E., Georgotas, A., 1987. Behavioral symptoms in Alzheimer's disease: phenomenology and treatment. J. Clin. Psychiatry 48 (Suppl. l), 9–15.

Rembach, A., Watt, A.D., Wilson, W.J., Villemagne, V.L., Burnham, S.C., Ellis, K.A., Group, A.R., 2014. Plasma amyloid-β levels are significantly associated with a transition toward Alzheimer's disease as measured by cognitive decline and change in neocortical amyloid burden. J. Alzheimers Dis. 40 (1), 95–104. https://doi.org/10.3233/JAD-131802.

Rivas, F., Diaz, L.A., Cardenas, V.M., Daza, E., Bruzon, L., Alcala, A., Tsai, T., 1997. Epidemic Venezuelan equine encephalitis in La Guajira, Colombia, 1995. J. Infect. Dis. 175 (4), 828–832. https://doi.org/10.1086/513978.

Rogers, D.C., Fisher, E.M., Brown, S.D., Peters, J., Hunter, A.J., Martin, J.E., 1997. Behavioral and functional analysis of mouse phenotype: SHIRPA, a proposed protocol for comprehensive phenotype assessment. Mamm. Genome 8 (10), 711–713. https://doi.org/10.1007/s003359900551.

Rogers, D.C., Peters, J., Martin, J.E., Ball, S., Nicholson, S.J., Witherden, A.S., Fisher, E. M., 2001. SHIRPA, a protocol for behavioral assessment: validation for longitudinal study of neurological dysfunction in mice. Neurosci. Lett. 306 (1–2), 89–92. https://doi.org/10.1016/s0304-3940(01)01885-7.

Ronca, S.E., Dineley, K.T., Paessler, S., 2016. Neurological sequelae resulting from encephalitic alphavirus infection. Front. Microbiol. 7, 959. https://doi.org/10.3389/fmicb.2016.00959.

Ronca, S.E., Smith, J., Koma, T., Miller, M.M., Yun, N., Dineley, K.T., Paessler, S., 2017. Mouse model of neurological complications resulting from encephalitic alphavirus infection. Front. Microbiol. 8, 188. https://doi.org/10.3389/fmicb.2017.00188.

Russo, M.V., McGavern, D.B., 2015. Immune surveillance of the CNS following infection and injury. Trends Immunol. 36 (10), 637–650. https://doi.org/10.1016/j.it.2015.08.002.

Salah, H., Abdel Rassoul, R., Medlej, Y., Asdikian, R., Hajjar, H., Dagher, S., Obeid, M., 2021. A modified two-way active avoidance test for combined contextual and auditory instrumental conditioning. Front. Behav. Neurosci. 15, 682927 https://doi.org/10.3389/fnbeh.2021.682927.

Schoneboom, B.A., Catlin, K.M., Marty, A.M., Grieder, F.B., 2000. Inflammation is a component of neurodegeneration in response to Venezuelan equine encephalitis virus infection in mice. J. Neuroimmunol. 109 (2), 132–146. https://doi.org/10.1016/s0165-5728(00)00290-3.

Sharma, A., Bhomia, M., Honnold, S.P., Maheshwari, R.K., 2011. Role of adhesion molecules and inflammation in Venezuelan equine encephalitis virus infected mouse brain. Virol. J. 8, 197. https://doi.org/10.1186/1743-422X-8-197.

Sharma, A., Knollmann-Ritschel, B., 2019. Current understanding of the molecular basis of Venezuelan equine encephalitis virus pathogenesis and vaccine development. Viruses 11 (2). https://doi.org/10.3390/v11020164.

Sochocka, M., Zwolinska, K., Leszek, J., 2017. The infectious etiology of Alzheimer's disease. Curr. Neuropharmacol. 15 (7), 996–1009. https://doi.org/10.2174/1570159X15666170313122937.

Sperling, R.A., Aisen, P.S., Beckett, L.A., Bennett, D.A., Craft, S., Fagan, A.M., Phelps, C. H., 2011. Toward defining the preclinical stages of Alzheimer's disease: recommendations from the National Institute on Aging-Alzheimer's Association workgroups on diagnostic guidelines for Alzheimer's disease. Alzheimers Dement 7 (3), 280–292. https://doi.org/10.1016/j.jalz.2011.03.003.

Stromberg, Z.R., Fischer, W., Bradfute, S.B., Kubicek-Sutherland, J.Z., Hraber, P., 2020. Vaccine advances against Venezuelan, eastern, and western equine encephalitis viruses. Vaccines (Basel) 8 (2). https://doi.org/10.3390/vaccines8020273.

Sung, P.S., Lin, P.Y., Liu, C.H., Su, H.C., Tsai, K.J., 2020. Neuroinflammation and neurogenesis in Alzheimer's disease and potential therapeutic approaches. Int. J. Mol. Sci. 21 (3) https://doi.org/10.3390/ijms21030701.

Tarawneh, R., Holtzman, D.M., 2012. The clinical problem of symptomatic Alzheimer disease and mild cognitive impairment. Cold Spring Harb. Perspect Med. 2 (5), a006148 https://doi.org/10.1101/cshperspect.a006148.

Targa Dias Anastacio, H., Matosin, N., Ooi, L., 2022. Neuronal hyperexcitability in Alzheimer's disease: what are the drivers behind this aberrant phenotype? Transl. Psychiatry 12 (1), 257. https://doi.org/10.1038/s41398-022-02024-7.

Taylor, A., Herrero, L.J., Rudd, P.A., Mahalingam, S., 2015. Mouse models of alphavirus-induced inflammatory disease. J. Gen. Virol. 96 (Pt 2), 221–238. https://doi.org/10.1099/vir.0.071282-0.

Taylor, K., Kolokoltsova, O., Ronca, S.E., Estes, M., Paessler, S., 2017a. Live, attenuated Venezuelan equine encephalitis virus vaccine (TC83) causes persistent brain infection in mice with non-functional alphabeta T-cells. Front. Microbiol. 8, 81. https://doi.org/10.3389/fmicb.2017.00081.

Taylor, K., Kolokoltsova, O., Ronca, S.E., Estes, M., Paessler, S., 2017b. Live, attenuated Venezuelan equine encephalitis virus vaccine (TC83) causes persistent brain infection in mice with non-functional αβ T-cells. Front. Microbiol. 8, 81. https://doi.org/10.3389/fmicb.2017.00081.

Tombaugh, G.C., Rowe, W.B., Chow, A.R., Michael, T.H., Rose, G.M., 2002. Theta-frequency synaptic potentiation in CA1 in vitro distinguishes cognitively impaired from unimpaired aged Fischer 344 rats. J. Neurosci. 22 (22), 9932–9940. https://doi.org/10.1523/JNEUROSCI.22-22-09932.2002.

Weaver, S.C., Ferro, C., Barrera, R., Boshell, J., Navarro, J.C., 2004. Venezuelan equine encephalitis. Annu. Rev. Entomol. 49, 141–174. https://doi.org/10.1146/annurev.ento.49.061802.123422.

Webster, S.J., Bachstetter, A.D., Nelson, P.T., Schmitt, F.A., Van Eldik, L.J., 2014. Using mice to model Alzheimer's dementia: an overview of the clinical disease and the preclinical behavioral changes in 10 mouse models. Front. Genet. 5, 88. https://doi.org/10.3389/fgene.2014.00088.

Williams, E.P., Xue, Y., Lee, J., Fitzpatrick, E.A., Kong, Y., Reichard, W., Jonsson, C.B., 2023. Deep spatial profiling of Venezuelan equine encephalitis virus reveals increased genetic diversity amidst neuroinflammation and cell death during brain infection. J. Virol. 97 (8), e0082723 https://doi.org/10.1128/jvi.00827-23.

Zhang, S., Wang, W., Li, J., Cheng, K., Zhou, J., Zhu, D., Xie, P., 2016. Behavioral characterization of CD36 knockout mice with SHIRPA primary screen. Behav. Brain Res. 299, 90–96. https://doi.org/10.1016/j.bbr.2015.11.027.

Zhou, J., Hormigo, S., Sajid, M.S., Castro-Alamancos, M.A., 2022. Caution influences avoidance and approach behaviors differently. J. Neurosci. 42 (30), 5899–5915. https://doi.org/10.1523/JNEUROSCI.1892-21.2022.

Zielinski, K., Werka, T., Nikolaev, E., 1993. Latency of the two-way avoidance response in rats: inhibition of delay. Acta Neurobiol. Exp. 53 (4), 535–545.